Gondwana Research 77 (2020) 238–259

Contents lists available at ScienceDirect

Gondwana Research

journal homepage: www.elsevier.com/locate/gr

Northward propagation of Andean genesis: Insights from Early Cretaceous synorogenic deposits in the Aysén-Río Mayo basin

Guido M. Gianni [a,b,*], César Navarrete [c], Andrés Echaurren [a], Marianela Díaz [d], Kristina L. Butler [e,f], Brian K. Horton [e,f], Alfonso Encinas [g], Andrés Folguera [a]

[a] IDEAN, Instituto de Estudios Andinos Don Pablo Groeber, UBA - CONICET. Departamento de Ciencias Geológicas, FCEN, Universidad de Buenos Aires, Argentina
[b] IGSV. Instituto Geofísico Sismológico Ing. F. Volponi. Universidad de Nacional San Juan, San Juan, Argentina
[c] Universidad Nacional de la Patagonia San Juan Bosco. Dpto. de Geología. Comodoro Rivadavia, Argentina
[d] Universidad Nacional de San Juan, Departamento de Geología, San Juan, Argentina
[e] Department of Geological Sciences, Jackson School of Geosciences, University of Texas at Austin, Austin, TX, USA
[f] Institute for Geophysics, Jackson School of Geosciences, University of Texas at Austin, Austin, TX, USA
[g] Departamento de Ciencias de la Tierra, Universidad de Concepción, Casilla 160-C, Concepción, Chile

ARTICLE INFO

Article history:
Received 26 March 2019
Received in revised form 21 July 2019
Accepted 22 July 2019
Available online 02 September 2019

Keywords:
Andes
Cretaceous contraction
Synorogenic deposits
Growth strata

ABSTRACT

Decoding the earliest orogenic stages in the Andes, the largest subduction orogen on Earth is fundamental to understanding changes in climate, drainage organization, and biodiversity in South America. Furthermore, it is crucial to unraveling the driving mechanism behind the initiation of orogeny. To track the earliest stages of Andean growth, we studied the Aysén/Río Mayo basin (ARB) in the North Patagonian Andes. The small degree of Cenozoic tectonic overprinting in this part of the Andes has allowed outstanding preservation of the deformational and sedimentary record of the earliest Andean deformation. In this study, we employ a multidisciplinary approach involving structural geology, sedimentology, geochronology, and provenance studies from the Early Cretaceous Apeleg Formation (~130–122 Ma) in the ARB and geochemical analysis of intrusive Cretaceous igneous rocks. Particularly, the recognition of syncontractional growth strata at several localities indicate a syntectonic origin for this unit and provide additional structural evidence of Early Cretaceous contraction in the North Patagonian Andes. Thus, the Apeleg Formation is interpreted as deposited during a contractional basin stage. Geochemical data from Aptian-Albian intrusive igneous rocks indicate that initial contraction emplaced over thinned crust likely inherited from the Jurassic extension in the ARB. This stage is then compared with a new synthesis of the earliest Cretaceous contraction along the Andes. This analysis reveals that the ARB likely holds the oldest post-Gondwanic synorogenic unit along the orogen and more significantly, that Andean birth was a diachronous process which propagated northward since the late Early Cretaceous. The latter findings have major implications for the evolution of the Andes and shed light into the driving mechanism behind initial orogeny.

1. Introduction

Over the last decades, studies documenting the earliest Andean orogenic stages after western Gondwana breakup, have shown evidence of shortening mostly since Late Cretaceous times (e.g. Dalziel et al., 1974; Mégard, 1984; Wilson, 1991; Fildani et al., 2003; Mpodozis et al., 2005; Arriagada et al., 2006; Jaimes and Freitas, 2006; Martin-Gombojav and Winkler, 2008; Tunik et al., 2010; Fennell et al., 2015; Gianni et al., 2015; Echaurren et al., 2016, 2017; Horton, 2008b; Horton et al., 2001; among others). At this time, the western South American margin experienced a change in subduction dynamics that lead to a shift in the tectonic regime from margin extension to backarc contraction (Vicente, 1970; Auboin et al., 1973). This stage has been classically linked to the Late Cretaceous separation from Africa at equatorial latitudes and the onset of the westward acceleration of South America (Fig. 1) (Dalziel et al., 1974; Mpodozis and Ramos, 1990; Coney and Evenchick, 1994). However, this hypothesis has been challenged in more recent studies. Faccenna et al. (2017) and Schellart (2017) used numerical modeling to suggest that the tectonic shift to contraction was triggered by subduction at lower mantle depth invigorating convection and ultimately driving plate margin contraction. Particularly the work of Faccenna et al. (2017) suggest that the Andean Cordillera main orogenic phase started at 60–50 Ma, after a long phase

* Corresponding author at: IDEAN, Instituto de Estudios Andinos Don Pablo Groeber, UBA - CONICET. Departamento de Ciencias Geológicas, FCEN, Universidad de Buenos Aires, Argentina.
E-mail address: guidogianni22@gmail.com (G.M. Gianni).

https://doi.org/10.1016/j.gr.2019.07.014
1342-937X/

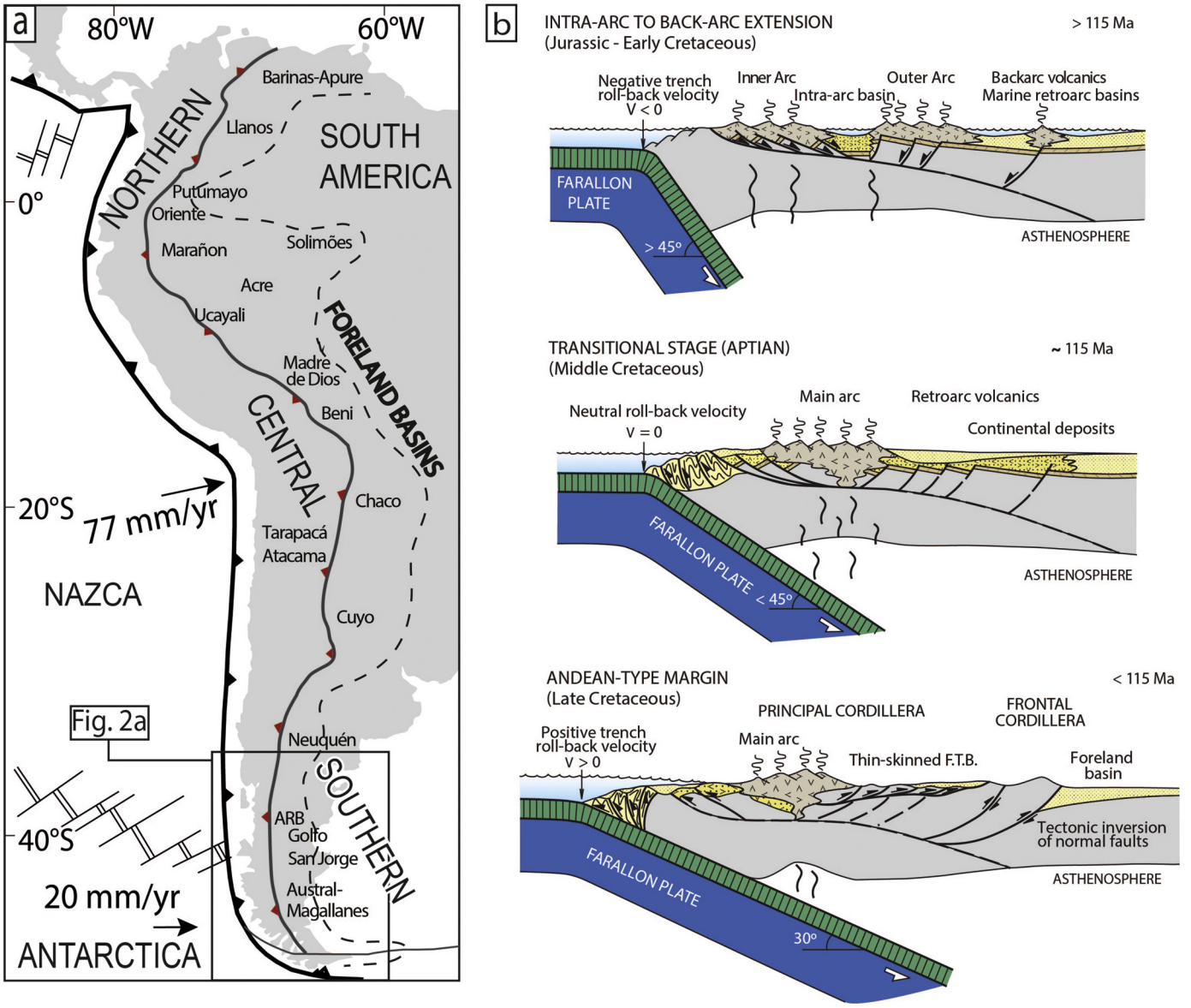

Fig. 1. a) This image shows the present tectonic setting of the Andean orogen and related foreland basins. Figure modified from Horton (2018a). b) Three main stages of Andean subduction during Mesozoic times exemplified by the tectonic evolution of the Southern Central Andes (33°S). Figure modified from Ramos (2009).

of westward drifting of South America. This hypothesis has been recently favored by Chen et al. (2019) based on the reconstruction of the Meso-Cenozoic Nazca plate subduction. Several geological studies addressing the most significant Paleogene to Neogene Andean deformation also assume that the Andes evolved after Late Cretaceous times (Oncken et al., 2006; Farías et al., 2010; Giambiagi et al., 2012; Decelles et al., 2015; Riesner et al., 2018, among many others).

Assessing the timing of the onset of the earliest Andean contractional stage is crucial to a better understanding of the geodynamic processes that initiated subduction orogeny. Such data are necessary to better comprehend the interactions between mantle-driven processes, topographic evolution, climate dynamics, biodiversity changes and Andean deformation (e.g. Lamb and Davis, 2003; Poulsen et al., 2010; Hoorn et al., 2010; Garzione et al., 2006; Nie et al., 2010; Baker et al., 2014; Armijo et al., 2015). Also, this information would benefit interpretations in studies assessing spatial and temporal trends in hydrology, drainage organization, and ecology conditions (e.g. Mulch et al., 2010).

Herein we address several fundamental questions regarding Andean evolution. Including, when and where did initial shortening precisely began? Was the onset of contraction coeval along the length of Andes, or did it propagate along strike? Uncertainties associated with these questions are often compounded by a limited geologic record of progressive constractional conditions, scarce documentation of active contractional structures contemporaneous to sedimentation, as well as limited constraints on depositional age and provenance.

The North Patagonian Andes offers a remarkable opportunity to evaluate the earliest Andean evolutionary stages. This segment has not been subjected to significant crustal shortening (~20–7 km, Orts et al., 2012; Echaurren et al., 2016; Gianni et al., 2017) and was not extensively overprinted by subsequent tectonic stages as the rest of the orogen (Fig. 2a). This allowed excellent preservation of the Mesozoic sedimentary record, which is advantageous to track early Andean growth. It is also noteworthy that one of the oldest Cretaceous angular unconformities in the orogen, dated between 121 and 118 Myr (Aptian) (Suárez et al., 2009a; Suarez et al., 2010), has been described in this area (e.g. Ramos, 1981a; Orts et al., 2012; Echaurren et al., 2017) (Fig. 2b). Synorogenic deposits linked to this primitive Andean stage remain undocumented. Some authors have suggested synorogenic deposition for the late Hauterivian-Aptian Apeleg Formation of the Aysén/Río Mayo Basin (ARB) (Aguirre-Urreta and Ramos, 1981) or the turbiditic Ingenieros Formation (Folguera and Iannizzotto, 2004) (Fig. 2b). However, subsequent studies pointed out the lack of structural and sedimentological evidence for the Early Cretaceous contraction and synorogenic deposition in these units (Bell and Súarez, 1997; Depine and Ramos, 2004; Demant and González, 2010; Suárez et al., 2009a, 2009b). Hence, most recent works have favored a model involving post-rift deposition during thermal subsidence of the ARB rifting stage.

In this study, we provide structural, sedimentologic, geochronologic, and provenance data, in support of a synorogenic character for the Apeleg Formation. We also obtained geochemical data from Early Cretaceous igneous rocks to estimate crustal thicknesses at this basin stage. Finally, the inferred deformation event is compared with a compilation of studies dealing with the onset of the Cretaceous contraction along the whole Andean Cordillera. This analysis reveals that the ARB holds the oldest post-Gondwanic foreland basin deposits in the orogen. The latter suggests the initiation of orogeny closely after southern South Atlantic opening, which has direct implications for competing models of Andean birth.

2. Geological framework

The Patagonian Andes are located in the southern sector of the active margin of western South America and are divided into the Northern and Austral Patagonian Andes at the Aysén triple junction (46°30′S) (Fig. 2a). North of this triple junction, the Nazca plate subducts beneath the North Patagonian Andes, while to the south the Antarctic plate is subducting under the Austral and Fuegian Andes.

During the Mesozoic, this region was subjected to regional extension related to the breakup of Western Gondwana producing several basins within the arc, retroarc and intraplate areas (Uliana et al., 1989). In the Early Jurassic, regional extension developed an NNW-trending retroarc marine/continental basin in Patagonia. In the North Patagonian Andes, deposits associated with this Early Jurassic basin are represented by volcaniclastic marine deposits of the Ostarena Formation (e.g. Suárez and Márquez, 2007) (Fig. 2b). From Middle to Late Jurassic times, several extensional depocenters developed associated with the eruption of extensive silicic volcanic rocks (Pankhurst et al., 2000). Subsequently, the last extensional stage took place between ~155 and 140 Myr during a southwestward shift of mesosilicic magmatism. This terminal extensional stage process produced the marine intraarc to backarc ARB (Ramos and Palma, 1983) (Fig. 2a).

The stratigraphy of the ARB comprises the volcanic calc-alkaline rocks of the Ibañez-Lago La Plata formations and the sedimentary and volcanic rocks of the Coyhaique Group (Suárez et al., 1996; Ramos, 1981a; Iannizzotto et al., 2004) (Fig. 2a). The latter includes, from base to top, the Toqui-Tres Lagunas, Katterfeld-Ingenieros and Apeleg formations. The Toqui and Tres Lagunas formations consist of shallow marine sedimentary deposits interbedded with pyroclastic rocks. Both units represent diachronic marine ingression. A Tithonian to Valanginian age for these units have been assigned based on ammonites and zircon U-Pb SHRIMP dating (see Suárez et al., 2009a and references therein). The Katterfeld Formation consists of black shales holding Valanginian to Hauterivian ammonites (Olivero and Aguirre-Urreta, 2002). This unit deposited in a restricted shelf environment that interfingered to the east with prodelta turbidites of the.

Ingenieros Formation (Iannizzotto et al., 2004). The youngest unit in the ARB is the Apeleg Formation, which is the focus of this study. This unit overlies and interfingers with the Katterfeld Formation (Ploszkiewicz and Ramos, 1987; González-Bonorino and Suárez, 1995). To the east, on the Argentinian side of the ARB, this unit mostly consists of deltaic sandstones and conglomerates (Ramos, 1981a; Hechem et al., 1993). In the western ARB in Chile, the Apeleg Formation presents facies characteristic of muddy flats and tidal sandbars interpreted as deposited in a shallow marine environment (Bell and Súarez, 1997). The upper sections of the Apeleg Formation record the final shallowing of the marine Aisén Basin. This is interpreted based on the description of basaltic volcanism and the formation of andesitic surtseyan tuff cones of the Baño Nuevo Volcanic Complex accumulated synchronously with the ultimate sedimentary stages of the Apeleg Formation (Demant and González, 2010) (Fig. 2b). Surtseyan tuff cones resulted from shallow level magma–water interaction during the emergence and growth of monogenetic volcanoes through standing water in the shallowing Aisén Basin (Demant et al., 2007).

The base of the Apeleg Formation is considered Hauterivian (~131–126 Ma; Aguirre-Urreta et al., 2019), based on the presence of *Favrella* sp. An early Aptian age is interpreted for the upper Apeleg Formation indicated by the ammonite *Tropaeum* or *Australiceras sp.* (Bell and Súarez, 1997; Suárez et al., 2009a and references therein). The latter is supported by radiometric ages of 122 and 121 Ma interfingered lavas and tuff cones in the top beds of this unit (three amphibole Ar/Ar ages and one U-Pb SHRIMP) obtained from interbedded volcanic rocks of the Baño Nuevo complex located 60 km to the southwest of the study area (Suarez et al., 2010) (Fig. 2b).

Following the Cretaceous marine regression, the ARB was covered in angular unconformity by subaerial calcalkaline volcanic rocks belonging

Fig. 2. a) Tectonic setting of the Patagonian Andes and the ARB (Aysén/Río Mayo Basin). Potential source areas to the Apeleg Formation are also shown. b) Stratigraphy of the ARB modified from Suárez et al. (2009a). c) Geological map from the study area based on Ploszkiewicz and Ramos (1987) and our own mapping. Abbreviations are LPF: Lago La Plata-Fontana, CBA: Lago General Carrera-Buenos Aires, LP: Lago Posadas, CHC: Chonos metamorphic complex, EAC: Eastern Andean complex, SCB: Subcordilleran Batholith, CPB: Central Patagonian Batholith.

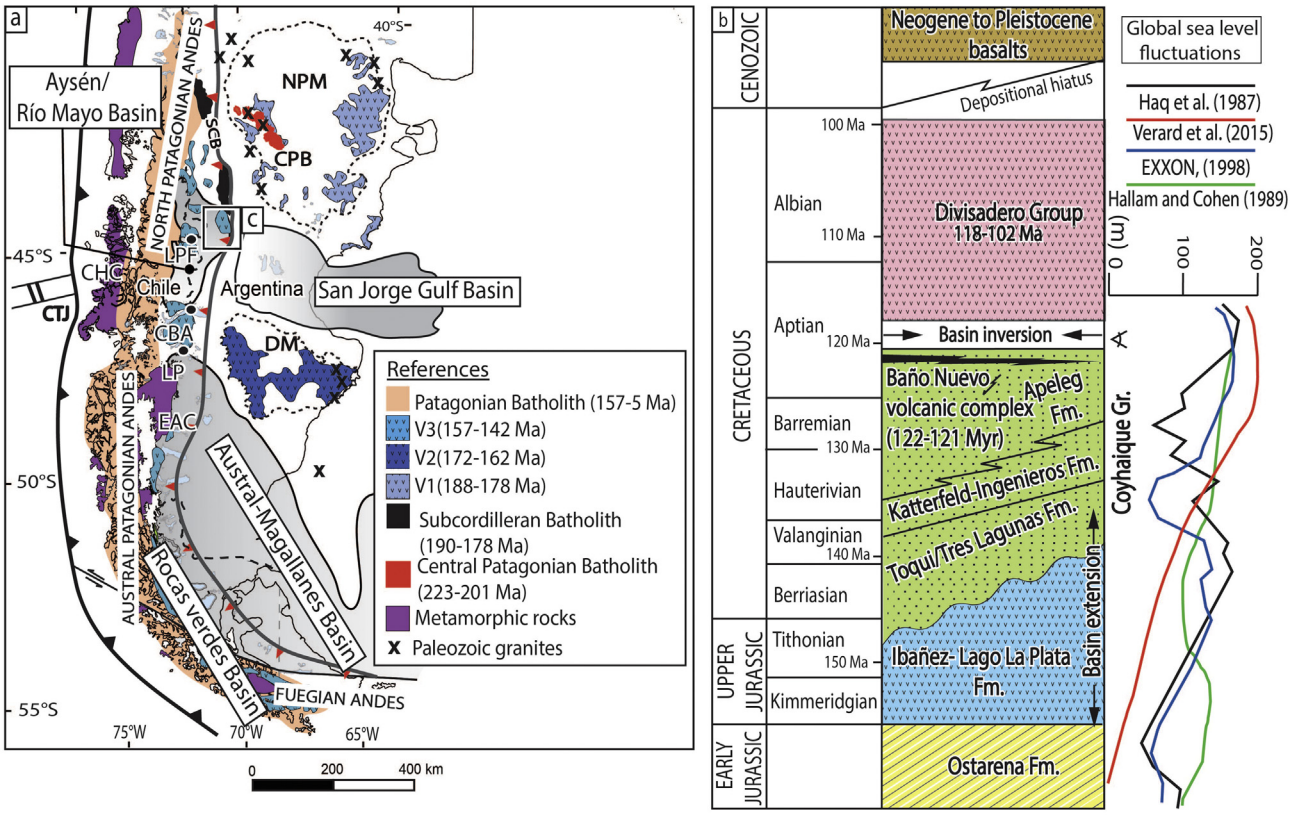
a
Aysén/
Río Mayo Basin
NORTH PATAGONIAN ANDES
SCEB
NPM
CPB
40°S
45°S
CTJ
CTC
TPF
Chile
Argentina
San Jorge Gulf Basin
CBA
DM
LP
EAC
50°S
AUSTRAL PATAGONIAN ANDES
Austral-Magallanes Basin
Rocas verdes Basin
FUEGIAN ANDES
55°S
75°W
70°W
65°W
0 200 400 km
References
Patagonian Batholith (157-5 Ma)
V3(157-142 Ma)
V2(172-162 Ma)
V1(188-178 Ma)
Subcordilleran Batholith (190-178 Ma)
Central Patagonian Batholith (223-201 Ma)
Metamorphic rocks
Paleozoic granites
b
CENOZOIC
Neogene to Pleistocene basalts
Depositional hiatus
CRETACEOUS
100 Ma
Albian
110 Ma
Divisadero Group 118-102 Ma
Aptian
120 Ma
Basin inversion
Baño Nuevo volcanic complex (122-121 Myr)
Apeleg Fm.
Barremian
130 Ma
Hauterivian
Katterfeld-Ingenieros Fm.
Valanginian
140 Ma
Toqui/Tres Lagunas Fm.
Berriasian
UPPER JURASSIC
Tithonian
150 Ma
Ibañez- Lago La Plata Fm.
Basin extension
Kimmeridgian
EARLY JURASSIC
Ostarena Fm.
Global sea level fluctuations
Haq et al. (1987)
Verard et al. (2015)
EXXON, (1998)
Hallam and Cohen (1989)
0 100 200 (m)
Coyhaique Gr.

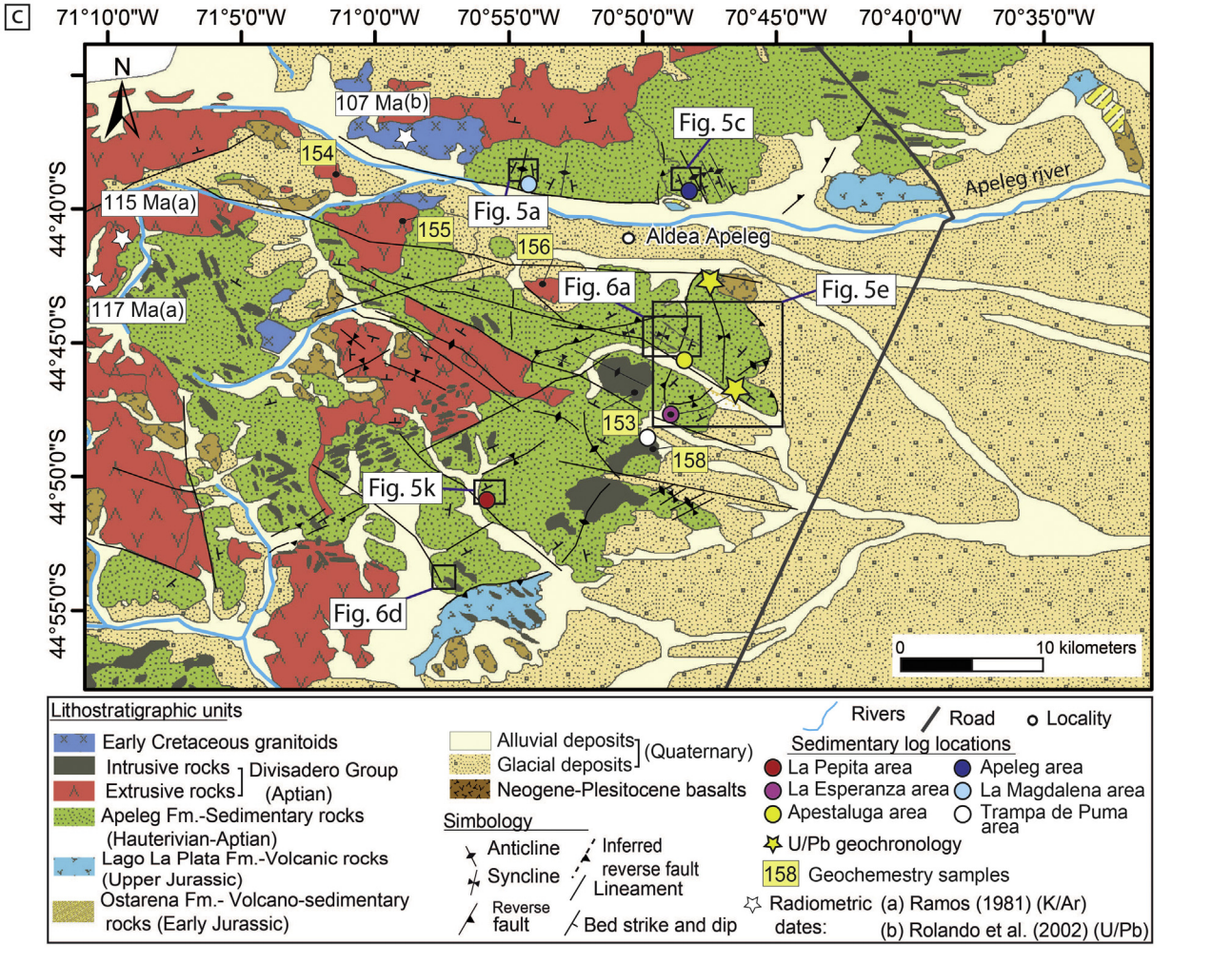
c
71°10'0"W
71°5'0"W
71°0'0"W
70°55'0"W
70°50'0"W
70°45'0"W
70°40'0"W
70°35'0"W
N
44°40'0"S
44°45'0"S
44°50'0"S
44°55'0"S
107 Ma(b)
154
115 Ma(a)
155
156
117 Ma(a)
153
158
Fig. 5c
Fig. 5a
Fig. 6a
Fig. 5e
Fig. 5k
Fig. 6d
Apeleg river
Aldea Apeleg
0 10 kilometers
Lithostratigraphic units
Early Cretaceous granitoids
Intrusive rocks
Extrusive rocks
Divisadero Group (Aptian)
Apeleg Fm.-Sedimentary rocks (Hauterivian-Aptian)
Lago La Plata Fm.-Volcanic rocks (Upper Jurassic)
Ostarena Fm.- Volcano-sedimentary rocks (Early Jurassic)
Alluvial deposits
Glacial deposits
(Quaternary)
Neogene-Plesitocene basalts
Simbology
Anticline
Syncline
Reverse fault
Inferred reverse fault
Lineament
Bed strike and dip
Rivers
Road
Locality
Sedimentary log locations
La Pepita area
Apeleg area
La Esperanza area
La Magdalena area
Apestaluga area
Trampa de Puma area
U/Pb geochronology
158 Geochemestry samples
Radiometric dates: (a) Ramos (1981) (K/Ar)
(b) Rolando et al. (2002) (U/Pb)

to the Divisadero Group (Ramos, 1981a; Suárez et al., 2009a) (Fig. 2b). The age of this unit has been constrained through U-Pb SHRIMP zircon dating that yielded ages between ~118 to 102 Myr (Pankhurst et al., 2003). The Divisadero Group is linked to a major magmatic stage associated with the Patagonian Batholith, which began its emplacement since Late Jurassic (see Echaurren et al., 2017 for a synthesis). The angular unconformity at the base of the Divisadero Group has been interpreted as evidence of one of the oldest Andean uplift stages (Iannizzotto et al., 2004). This contractional event has been constrained to the 121–118 Myr time interval (Aptian) based on geochronological data from the Apeleg Formation and the Divisadero Group (Suárez et al., 2009a) (Fig. 2b). In the study area, this magmatic stage is also represented by subvolcanic bodies such as sills and dikes and granitoids intruding the Apeleg Formation (Ploszkiewicz and Ramos, 1987) (Fig. 2c). Finally, a Late Cretaceous contractional episode is associated with the tectonic emplacement of the Patagonian Batholith in the Lago La Plata-Fontana fold belt (Ramos and Palma, 1983; Iannizzotto et al., 2004) (LPF in Fig. 2a).

3. Methodology

3.1. Sedimentology of the Apeleg Formation

To understand the depositional environment of the Apeleg Formation, we describe sedimentary sections in different structures of the external sector of the LPF (Fig. 2c). Beds were divided into facies taking into account lithologic composition, sedimentary structures, and facies geometry. These sections provided the framework to sedimentologic data, conglomerate clasts counts, petrographic thin sections, and detrital zircon (U-Pb) sampling. Also, we measured 270 paleocurrent orientations at 29 sites in tabular cross-stratified sandstones. These were later restored for bedding tilt (see Table S1 in supplementary data for the complete dataset).

3.2. Growth strata detection

To study growth structures in the Apeleg Formation, we carried out direct dip measurements, recorded changes in bed thickness, and identified intraformational angular unconformities (Riba, 1976). Also, we registered the presence of sedimentary onlaps towards fold hinges or faults on contractional structures. This methodology is suitable to distinguish distinctive bed fanning in growth strata from drag folds forming local flexures in homoclinal beds near normal or contractional faults in the hanging wall (e.g. Gianni et al., 2018a). To discriminate contractional fanning structures from those developed during extension, such as tectonic rollover growth-strata folds (e.g. Finch et al., 2004), growth strata associated with fault-tip monoclines (Gawthorpe and Hardy, 2002) or delta-related synsedimentary normal faulting (e.g. Bhattacharya and Davies, 2001); we only studied sections closely associated with structures with clear contractional kinematics. Moreover, as mesoscale normal faults in synextensional deposits are often preserved even after strong inversion of the depocenter bounding normal faults (Bechis et al., 2010; Giambiagi et al., 2011), determination of their absence at all localities was used as an additional criterion to discard a synextensional origin for growth strata geometries. When possible we recognized typical syntectonic geometries formed during thrusting such as syncline-growth structures (e.g. Hong et al., 2007). We analyzed areas devoid of pervasive shearing to prevent mistaking syntectonic deposits with strata divergence and thickening caused by potential trishear folding. Furthermore, we combined our analysis of growth strata with paleocurrent determinations which provide information about flow directions and related modifications during the development of contractional structures (Burbank et al., 1996).

3.3. Provenance analysis

In order to determine potential sediment source areas in the Apeleg Formation, we present data from conglomerate and sandstone compositions, and carried out U-Pb zircon geochronology.

For conglomerate composition we conducted clasts counts at 9 sites using 30 × 30 cm grids on outcrops of pebble to cobble conglomerates. Clasts were identified according to rock type, mineralogy, and grain size.

For sandstone composition we conducted petrographic analyses on 21 samples of sandstones from the Apeleg Formation (refer to tables S2 and S3 in supplementary data for the complete dataset). We obtained thin sections for each sample and carried out 300 grains point-counting using the Gazzy-Dickinson method (Gazzi, 1966; Zuffa, 1985).

For U-Pb zircon geochronology we collected a sample from the base of the La Esperanza section (sample APG 152, location in Fig. 2c; see supplementary table S5 in material for the complete dataset). Heavy-mineral concentrates of the <350 μm fraction were separated using traditional techniques at ZirChron LLC. Zircons from the non-magnetic fraction were mounted in a 1-in. diameter epoxy puck and slightly ground and polished to expose the surface and for laser ablation analyses. After cathode-luminescence (CL) imaging at University of Idaho, the LA-ICP-MS U-Pb analyses were carried out at Washington State University using a New Wave Nd: YAG UV 213-nm laser coupled to a Thermo Finnigan Element 2 single collector, double-focusing, magnetic sector ICP-MS. Operating parameters and procedures are similar to those of Chang et al. (2006). Laser spot size and repetition rates were 30 μm and 10 Hz, respectively. He and Ar carrier gases delivered the sample aerosol to the plasma. Each analysis consists of a short blank analysis followed by 250 sweeps through masses 202, 204, 206, 207, 208, 232, 235, and 238, taking approximately 30 s. Time-independent fractionation was corrected by normalizing U/Pb and Pb/Pb ratios of the unknowns to the zircon standards (Chang et al., 2006). U and Th concentrations were monitored by comparing to NIST 610 trace element glass. Two zircon standards were used: Plesovice, with an age of 338 Ma (Sláma et al., 2008) and FC-1, with an age of 1099 Ma (Paces and Miller, 1993). Uranium lead ages were calculated and plots generated using Isoplot (Ludwig, 2003). To determine the maximum depositional ages we identify the youngest age group (more than three) overlapping within the error (Gehrels et al., 2006). Then, we calculated an age from this group using the Tuffzirc algorithm of Ludwig (2003) and age errors were reported using the quadratic sum of the analytical error plus the total systematic error for the set of analyses (Gehrels et al., 2008).

An additional medium-grained sandstone sample was collected from the Apeleg Formation near the town of Apeleg (19APL01; location in Fig. 2c; see supplementary table S5 in material for the complete dataset). Standard zircon isolation methods were used including rock crushing and grinding, as well as hydraulic, heavy-liquid density and magnetic separation at the University of Texas at Austin following the mineral separation guidelines of the University of Arizona LaserChron Center (Gehrels et al., 2006). Zircon grains were poured into 20 μm thick epoxy mounts, polished and imaged at the University of Arizona LaserChron. Zircon U-Pb geochronological analyses were conducted over two sessions at the Arizona LaserChron Center by laser ablation inductively coupled plasma mass spectrometry (LA-ICPMS) on the Element2 HR ICMPS following the analytical techniques of Gehrels et al. (2006, 2008) and Gehrels and Pecha (2014). Backscatter electron images were used to pick analytical spots at random. Spots were ablated with a beam diameter of 20 μm, a laser wavelength of 193 nm, at a repetition rate of 8 Hz, and a fluence of ~5 J/cm^2. Age calibration standards include: Sri Lanka, FC-1, and R33. Uncertainties of 1–2% (1σ error) are reported for $^{206}Pb/^{238}U$ and $^{206}Pb/^{207}Pb$ ages. We report $^{206}Pb/^{238}U$ ages for zircons younger than 900 Ma and $^{206}Pb/^{207}Pb$ ages for zircons older than 900 Ma. Individual analyses were filtered by >20% discordance, >5% reverse discordance, or 10% internal uncertainty. Ages and associated uncertainties are presented in the following section as

histograms and probability density plots (Sharman et al., 2018), enabling the discrimination of key age populations and visual graphical comparison. Age peaks are defined by three or more zircon grains with individual ages that overlap at the 1σ level.

3.4. Geochemistry

To quantify crustal thickness in Early Cretaceous times and to determine the nature of the magmatism in the study area we analyzed Aptian igneous rocks from the Divisadero Group intruding the Apeleg Formation (Fig. 2c). We selected five samples from the Divisadero Group for a geochemical analysis (see the precise locations and table S4 in supplementary data), corresponding to several granodioritic to tonalitic intrusives and a subvolcanic rhyolitic body. The totality of collected samples corresponds to fresh rocks. The analyses were performed by Acmelabs – Bureau Veritas, Vancouver, Canada. Major, trace and rare earth element (REE) contents were determined ICP/ICP MS (Inductively Coupled Plasma Mass Spectrometry). For complete details in the procedure followed by the laboratory refer to code LF202 in www.acmelab.com. For metallic elements, a solution was made with aqua regia and then an ICP-ES/MS (Inductively Coupled Plasma-Emission Spectrometer/Mass) analysis.

4. Results and interpretations

4.1. Sedimentology

We studied six sedimentary sections (Apeleg, La Magdalena, La Esperanza, Apestaluga, La Pepita and Trampa de Puma areas) outcropping related to different contractional structures (Fig. 2c). In the examined areas, this unit mainly consists of pale green and brown sandstone, conglomeratic sandstone and conglomerate. The unit is locally intruded by dacitic to rhyolitic dikes at several localities (Fig. 3). We identified eight lithofacies in the Apeleg Formation (Table 1) (Fig. 4). 1) Black mudstones and shales (F). This facies only appears at the Trampa de Puma section and presents bed thickness ranging from 15 to 400 cm (Fig. 3). It is interpreted as reflecting suspension settling in waning flow conditions. 2) Horizontally stratified sandstones (Sh). This facies consists of medium- to coarse- and sometimes pebbly sandstones with 1–40 cm bedding, occasional coarsening upward, and hosting oriented petrified logs. It is interpreted as deposited under upper flow regime conditions. 3) Massive sandstones (Sm). This facies is characterized by a 30–80 cm bed thickness, sharp basal contacts and occasional thinning upward. This is interpreted as related to rapid deposition by sheet or sediment gravity flows. 4) Planar cross-stratified sandstones (Sp). This facies forms laterally continuous beds with a set thickness between 50 and 200 cm with occasional burrows and oriented petrified logs. Fluid escape and synsedimentary deformational structures are locally observed. It is interpreted as related to the migration of large 2-D dunes. 5) Hummocky cross-stratified sandstones (HCS). This facies occurs only occasionally and presents undulating cross-beds and low-angle truncations (Fig. 3). This is interpreted as the result of storm waves and deposition in the lower shoreface and transition zone between fairweather wave-base and storm wave-base. Particularly, at the La Pepita area, this facies appears interbedded with highly bioturbated fine-grained massive sandstones showing *Planolites sp., Gyrochorte sp., Asteriacites lumbricales, Ophioichnus aysenensis*, which characterized the *Cruziana* ichnofacies (Fig. 4). This ichnofacies has been previously identified in the Apeleg Formation and described in detail by Bell (2004). 6) Clast-supported and planar cross-stratified conglomerates (Gcp). This facies is interpreted as deposited in longitudinal bars. 7) Clast-supported and massive conglomerates (Gcm) likely deposited from sheetfloods and clast-rich debris flows. 8) Matrix-supported and massive conglomerates (Gmm) interpreted as deposited by debris flows.

We classify these facies into three main facies associations (Table 2). Facies association S1 makes up most of the analyzed sections in the Apeleg Formation. It consists of medium- to coarse-grained sandstones with planar cross-stratification (Sp) and horizontal stratification (Sh) as well as occasional beds with HCS. Paleocurrent measurements in Sp mostly indicate unimodal paleoflows showing low dispersion and main directions to the W and WNW except for the Apestaluga area with directions roughly to the E (Fig. 3). We interpret this facies association as indicating deposition in a delta-front from rapidly decelerating unidirectional flows in distributary mouth-bar environments. The presence of HCS is interpreted as indicating sporadic reworking of sandy delta-front lithofacies by storm processes. Preservation of structures formed by unidirectional flows could have been favored by high rates of deposition and rapid burial in this setting (Bhattacharya, 2006). This interpretation is compatible with the occurrence of stressed trace fossils of *Cruziana* ichnofacies (Bell, 2004) at La Pepita area and the presence of glauconite (3.77–0.45%) in samples from Sp, Sh and HCS lithofacies (see supplementary table S2). Facies association S2 only appears at Trampa del Puma section. This contains medium-grained massive sandstones of facies Sm intercalated with dark shales and mudstones of facies F (Fig. 4). At this locality, Sm contains abundant mudstone rip-up clasts (Fig. 4e). This association is interpreted as deposited by turbidity currents in a prodelta environment where facies Sm are interpreted as Ta Bouma cycles.

The G1 association occurs mostly separated from S1 and S2 and is mainly present to the west of the study area at La Magdalena area. This facies association is composed of massive and planar cross-bedded conglomerates of Gcp, Gcm and Gmm and massive sandstones of Sm lithofacies. This is interpreted as debris or hyperconcentrated flows on an alluvial fan. (Figs. 2c and 3).

We interpret the sedimentary environment of the Apeleg Formation in the analyzed area as deposited in a deltaic setting. Only locally an alluvial environment is interpreted to the west at La Magdalena area possibly related to deposition in an upper delta plain setting where river processes dominate (Bhattacharya, 2006). According to the paleoflow determinations, this deltaic system could have been fed mostly from the E and ENE and more locally from the W (Apestaluga area) (Fig. 3). These interpretations are in harmony with previous findings in neighboring areas in the eastern sector of the ARB interpreting a mostly deltaic environment in the Apeleg Formation (Scasso, 1989; Hechem et al., 1993; González-Bonorino and Suárez, 1995). According to Scasso (1987), this deltaic system was fed by fluvial systems represented by the Valanginian-Aptian Puesto Albornoz and Manantial Pelado formations outcropping to the east of the study area.

4.2. Evidence of syncontractional deposition: growth strata in the Apeleg Formation and structural evidence of Cretaceous contraction

The general structure in the study area is characterized by the presence of two sets of structures. A WNW- and WSW-striking regional-scale fractures and several WNW- WSW- and ~N-striking thrust and folds with a wavelength of ~1–2 km (Ploszkiewicz and Ramos, 1987) (Fig. 2c). According to Folguera and Iannizzotto (2004), the structure of the North Patagonian Andes in this area is related to basin inversion of previous Late Jurassic-Neocomian depocenters of the ARB. However, as the study area lacks seismic reflection data and synrift units are not well exposed, we therefore cannot infer the deep structure and related deformation mechanism.

In this work, syncontractional growth strata in the Apeleg Formation were detected in numerous structures that constitute the orogenic front of the North Patagonian Andes at the study area. In the western sector, at the la Magdalena area, we observe strata dip variations from 35° to 12–9° to the NE, sedimentary wedging and bed thickness changes in the forelimb of an N-striking and eastward verging anticline (Figs. 2c and 5a, b).To the east, we also found growth strata geometries in the vicinity of the Apeleg area (Fig. 2c). In this sector, a westward verging and

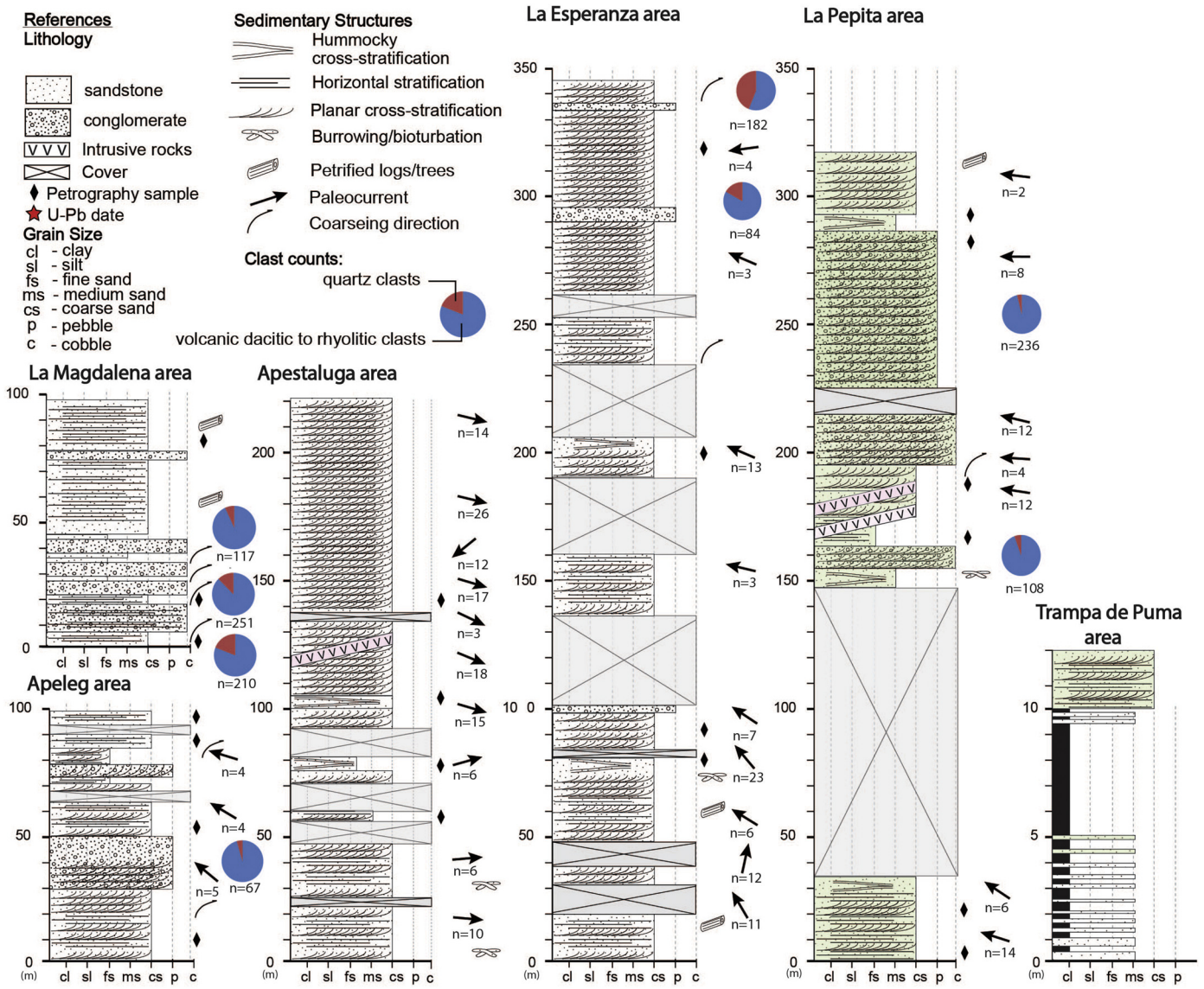

Fig. 3. Measured stratigraphic sections in the Apeleg Formation at the study area showing lithologies, sedimentary structures, paleocurrents, conglomerate clast compositions. Sandstone petrographic sample locations and U/Pb sample location are also shown. For the location of the sections see Fig. 2c.

Table 1
Description and interpretation of lithofacies.

Facies code	Description	Process interpretation
F	Organic-rich mudstones and shales with 15 cm-4 m bed thickness	Suspension-settling in waning flow conditions in turbidity currents
Sh	Medium- to coarse-grained and sometimes pebbly sandstone; horizontally stratified with eventual burrows; laterally continuous, sharp-basal contacts to slightly erosional; 1–40 cm bed thickness; rare gravel, occasional coarsening upward; petrified trunks (up to 50-cm diameter)	Planar bed flow; upper flow regime
Sm	Medium- to coarse-grained sandstone; massive; 30–80 cm bed thickness; sharp basal contacts; occasional thinning upward.	Rapid deposition by sediment gravity or sheet flow
Sp	Coarse-grained and pebbly sandstone with occasional pelitic clasts, planar (tangencial) cross-stratification, set thickness 50–200 cm; eventual burrows; laterally continuous, petrified trunks	Migration of large 2D ripples (dunes) under moderately powerful, unidirectional channelized flows.
HCS	Medium- to coarse- grained sandstone with hummocky cross-stratification,; 15–30 cm bed thickness, locally interfingered with bioturbated fine-sandstone holding *Planolites sp., Gyrochorte sp., Asteriacites lumbricales, Ophioichnus aysenensis*	Storm beds deposited in a shallow marine setting in the outer shoreface and transition zone between fairweather wave-base and storm wave-base.
Gcp	Subangular to rounded pebble to cobble polymictic conglomerate, clast-supported, planar cross-stratified	Migration of longitudinal bars
Gcm	Subangular to rounded pebble to cobble polymictic conglomerate, poorly sorted, clast-supported, structureless, massive, poorly organized	Deposition from sheetfloods and clast-rich debris flows
Gmm	Subangular to rounded pebble polymictic conglomerate, matrix supported, disorganized, poorly sorted	Hyperconcentrated flow or debris flow

NW-striking anticline depicts fanning strata from 30° to 6° roughly to the west and a systematic thinning of the sedimentary packages towards the anticline hinge (Figs. 5c, d). The central sector of the study area presents a series of thrusts and folds with a variable strike (Fig. 2c). This zone is characterized by the presence of the El Amigo syncline, which depicts a change in strike from NNW in the northern extreme to SSW in the southern area (Fig. 5e). Based on the documentation of opposite dipping fanning strata on both syncline flanks, this structure is interpreted as a syncline growth (Fig. 5e). The western flank, at the Apestaluga location, is linked to an east-verging thrust to the west and presents growth geometries with eastward dipping strata variations from 30° to 3° (Fig. 5f). To the south, this same structure propagates an anticline which presents overturned fanning strata that define a dip variance of ~115° (Fig. 5g). Beds at the base present strata dips ranging from 73 to 53° to the NW, and to the top of the section, beds depict dips variations from 22 to 12° to E (Fig. 5g). Notably, up-section attenuation in bed deformation over the frontal limb of this structure follows typical geometries found in syncontractional growth folds (e.g. Suppe et al., 1997). The eastern flank, at the La Esperanza area, describes growth strata with beds presenting systematic thinning towards the SSE and dip variations from 40° to 4° to the NNW (Fig. 5h,i, j). In the southernmost sector of the study area, a large-scale growth structure is identified at the La Pepita area (Fig. 2c). This structure depicts an internal syntectonic angular unconformity within the succession, sedimentary onlaps and systematic thickness variations, and fanning strata from 40° to 7–3° to the NW (Fig. 5k).

All the localities with growth strata present fanning directions that are compatible with paleoflow determinations. The only exception is the La Magdalena area that lacks structures from where to obtain paleocurrent measurements (Fig. 3 and 5c, e, k).

Particularly interesting is the El Amigo syncline growth at the Apestaluga and La Esperanza areas, where we determined a convergent paleoflow towards the syncline axis. This highlights the influence of this contractional structure on the local paleoflow during deposition of the Apeleg Formation and further supports the syncontractional origin of the growth strata.

Overall, the fact that normal faulting or the evidence of reactivated faults at macro- and meso-scale in syntectonic deposits (e.g. Bechis et al., 2010; Giambiagi et al., 2011) is absent at all localities as well as the fact that most growth geometries are directly related to contractional structures preclude linking growth strata to an extensional setting. Additionally, no growth normal-faulting has been observed that could help linking growth strata genesis to sedimentary dynamics in deltaic environments (Bhattacharya and Davies, 2001). Furthermore, described geometries associated with overturned folds terminating in gently dipping beds as well as opposing dipping growth strata associated with the El Amigo syncline differ from classical large-scale clynoform geometries described in Gilbert-type deltas.

Independent evidence suggesting that these structures began to form in Early Cretaceous times is derived from cross-cutting structural relationships between the Divisadero Group (Aptian-Cenomanian) (Ploszkiewicz and Ramos, 1987) and the Apeleg Formation. This is illustrated by the presence of relatively undeformed rhyolitic dikes at the Apestaluga area and Early Cretaceous quartz veins (Domínguez, 1981; Lanfranchini et al., 1999) at La Pepita area intruding previously formed thrusts and syncline folds (Fig. 6).

4.3. Provenance of the Apeleg Formation

4.3.1. Conglomerate composition

Conglomerates were classified into two groups: volcanic silicic rocks (dacite and rhyolite) and quartz clasts. Conglomerates from the Apeleg Formation show >80% volcanic clasts and more limited quartz (Fig. 3).

Volcanic clasts composition indicates sediment derived from two potential sources, both linked to the Chon Aike Magmatic Province in Patagonia (Pankhurst et al., 2000). One located to the west and around the study area known as the V3 stage, which is represented by the Lago La Plata Formation (Fig. 2a) and the other to the east, associated with the V1 and V2 stages (Marifil Formation and Bahia Laura Group) in the foreland sector. In particular, the latter volcanic source is supported by paleocurrent data. On the other hand, quartz detritus could have originated from multiple metamorphic sources such as the late Paleozoic Eastern Andean Complex (EAC) to the south or the Triassic Chonos Metamorphic Complex (CMC) to the west or metamorphic Paleozoic basements located to NE and SE (North Patagonian Massif and Deseado Massif, respectively) (Fig. 2a).

4.3.2. Sandstone composition

Grain categories are outlined in Table 3, whereas results are plotted in ternary diagrams (Fig. 3a, b, and c; Folk et al., 1970; Dickinson, 1983). Analyzed sandstones are in all cases medium-to-coarse grained. Quartz is abundant; being monocrystalline quartz (Qm) and Polycrystalline quartz (Qpg) the most frequent varieties (15% of total framework grains). K-feldspar is more frequent than plagioclase (19% vs 0.44%). The lithic fraction is largely dominated by acidic volcanic fragments (27% of total framework grains) with minor contributions of plutonic fragments (7.7%). Glauconitic grains are subordinated (0.78%), although their content is as high as 3.77% in two of the analyzed samples. According to Folk et al. (1970) classification scheme, these arenites classify as lithoarenites and feldspathic lithoarenites, with variable contents of

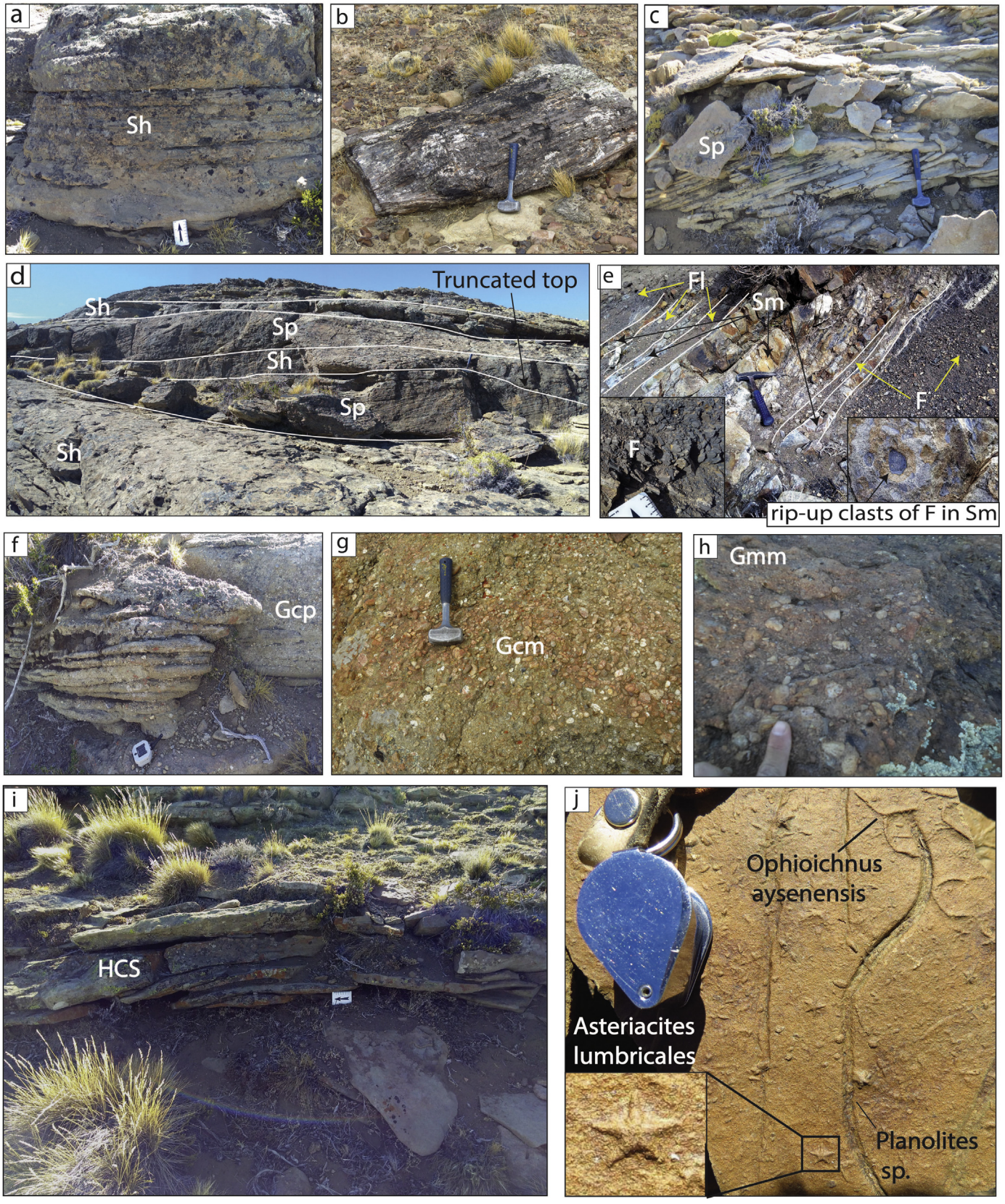

Fig. 4. Photographs of sandstone and gravel lithofacies from the Apeleg Formation in the study area. a) Horizontally stratified sandstones (Sh). b) Petrified logs in Sh. c) Planar cross-stratified sandstones (Sp). d) Field photograph of S1 facies association. e) Field photograph of S2 facies association of interbedded massive sandstones (Sm) and shales (F). f) Planar cross-bedded conglomerates (Gcp). g) Massive clast-supported conglomerates (Gcm). h) Massive matrix-supported conglomerates (Gmm). i) Sandstones with hummocky cross-stratification (HCS). j) Bioturbated sandstones with marine trace fossils characteristic of the *Cruziana* ichnofacies.

Table 2
Description and interpretation of facies associations.

S1: Cross-stratified and bedded sandstones	Sh, Sp, HCS	Deposition in terminal distributary channels and mouth bars in a delta front environment with occasional storm reworking
S2: Mudstones and shales with interbedded massive sandstones	F, Sm	Prodelta
G1: Cross-stratified and massive conglomerates with interbedded massive sandstones	Gcp, Gcm, Gmm, Sm	Alluvial fan

quartz (Fig. 7a). This is coherent with petrographic observations, where volcanic fragments constitute the majority of framework grains, with minor K-feldspar, and quartz. Dickinson (1983) QFL diagram indicate multiple sources for these sediments. A volcanic source (Transitional and Dissected Arc) is interpreted due to the high abundance of volcanic fragments (Fig. 7b). On the other hand, a Recycled Orogen source is probably linked to high total quartz contents. The QmFLt diagram also shows multiple detrital sources. The volcanic source is again dominant (Arc fields), whereas a Recycled Lithic-to-Transitional Orogen constitutes a minor source, as evidenced by the samples plotted in those fields and the Mixed Sources Field (Fig. 7c).Overall, these arenites are mainly composed of volcanic lithic fragments, monocrystalline quartz, polycrystalline quartz, and K-feldspar. In some cases glauconitic grains are abundant.

Similar to the conglomerate composition, the most likely volcanic sources for these sediments are the V3 stage in the west or the V1 and V2 stages in the east, which all belong to the Chon Aike magmatic province (Fig. 2a). These source areas would have contributed to volcanic lithic fragments and monocrystalline quartz grains. A second source area corresponds to a recycled orogen, which probably was the source of both, polycrystalline quartz and K-feldspar. The latter could have originated from metamorphic rocks of the EAC in the Andes to the south or CMC in the west (Fig. 2a).

4.3.3. Detrital zircon U-Pb geochronology

4.3.3.1. Maximum depositional age of the Apeleg Formation. Sample 19APL01 yielded two youngest grains which overlap within error (Fig. 7d). These results suggest a maximum depositional age of ~130–124 Ma, in agreement with the late Hauterivian to Aptian fossil record described in this unit (see Suárez et al., 2009a). Sample APG-152 was collected from the base of the sedimentary section at the La Esperanza area. This sample yielded a single youngest grain of ~150 Ma. The youngest grain population is not representative of the depositional age of the Apeleg Formation, perhaps due to a lower number of grains analyzed.

4.3.3.2. Provenance of the Apeleg Formation. The spectrum of the >360 zircon U-Pb ages obtained from two detrital sandstone samples fall dominantly between ~150 Ma and 333 Ma (see supplementary table S5for a complete dataset) (Fig. 7d). The distribution of these ages present bimodal graphical peaks at ~183–182 Ma and ~159–155 Ma (Fig. 7d). There are minor age populations of Carboniferous (~333–311 Ma), Permian (~292–258 Ma), and Triassic (~248–211 Ma) age grains.

Two potential sediment source zones could have supplied populations represented by these age peaks. In the North Patagonian Andes, immediately to the north of the study area, a possible source is I-type calc-alkaline intrusives of the Subcordilleran batholith (SCB) (190–178 Ma) (Rapela et al., 2005) (Fig. 2a). Alternatively, detritus could have been delivered from the Patagonian interior to the east, from the silicic volcanic rocks of the Jurassic V1 stage (188–178 Ma) of the Chon Aike Magmatic Province (Pankhurst et al., 2000). The Patagonian interior has two potential sediment source regions characterized by the V1 volcanic stage, one in the North Patagonian Massif (NPM) (Marifil Formation) to the NE and the other to the ENE from the Lonco Trapial Group (Fig. 2a). Both sources, the SCB, and the V1 may have contributed to the Apeleg Formation. However, the mostly westward-directed paleocurrents and the predominance of volcanic clasts in conglomerates and the sandstone petrographic analyses suggest that the V1 (Marifil and/or Lonco Trapial Group) was the dominant source (Figs. 3 and 7). Futhermore, Butler et al. (2019) recently suggested that the SCB began supplying sediment to wedgetop and foreland depocenters in the middle-late Miocene coincident the main phase of fold-thrust belt development. It is noteworthy that several previous studies also demonstrate the significance of the V1 sediment source in Aptian-Albian units in different Patagonian basins (e.g. Navarro et al., 2015; Ghiglione et al., 2015; Malkowski et al., 2017; Sickmann et al., 2019). The smaller age population between ~160–150 Ma most likely corresponds to the V3 volcanic stage (157–142 Ma), exposed along the Andes forming the basement to the Coyhayque Group in the ARB (Ramos, 1981a) (Fig. 2a). Carboniferous to Triassic zircons could have been supplied from Paleozoic–Triassic metamorphic complexes associated with the proto-Andean convergent margin as seen in Cretaceous units from the Austral-Magallanes Basin (Malkowski et al., 2017) (Fig. 2a). Alternatively, Carboniferous and Permian zircons could have been delivered from the northeast from late Paleozoic (~320–250 Ma) subalkaline granitoids in the northern and western sector of the North Patagonian Massif (Ramos, 2008) (Fig. 2a). Triassic zircons may also have had an eastern source corresponding with granitoids from the Central Patagonian Batholith (CPB) (223–201 Ma; Rapela et al., 2005) (Fig. 2a).

4.3.4. Geochemistry of Divisadero magmatism

We analyzed Aptian igneous rocks from the Divisadero Group intruding the Apeleg Formation to obtain an estimation of the Early Cretaceous crustal thickness and to determine the nature of the magmatism in the study area (Fig. 2c). Age determinations (K/Ar and U/Pb) for this unit in the study area have yielded ages between 117 and 107 Myr (Ramos, 1981a; Rolando et al., 2002) (Fig. 2c). Thus, geochemical data from these rocks can give us information regarding the crustal thickness immediately after the contractional stage recorded from growth strata and by cross-cut structural relations (Figs. 5 and 6).

We present major and trace element composition of four intrusive rocks and one lava dome (see table S5 in the supplementary information for the complete dataset). We compared these samples with a published geochemical compilation of the Divisadero Group from Echaurren et al. (2017) which is representative of the background regional trend. In terms of composition these rocks classify as granites and granodiorites with a high silica content (SiO_2 68.13–77.84 wt%. Fig. 8a), low MgO, $Fe_2O_{3(t)}$ and TiO_2 contents (0.22–1.28, 1.6–3.57 and 0.07–0.53 wt%, respectively) and Al_2O_3 contents of 13.1–16.45 wt%. All samples show a clear calc-alkaline and high-K calc-alkaline affinity in the K_2O vs. SiO_2 diagram (Peccerillo and Taylor, 1976. Fig. 8b), and values of alumina saturation index predominantly below of 1.1 (Fig. 8c), except for one sample presenting higher values. The latter allows classifying these Cretaceous rocks as related to a metaluminous to peraluminous magmatism (Shand, 1943), with a predominance of I-type granites (Chappel and White, 2001) (Fig. 8c). On the other hand, the trace multielemental diagram normalized to a primitive mantle (McDonough and Sun, 1995) shows an enrichment of Th, U and Pb, and negative anomalies of Nb, Ta and Ti (Fig. 8d), which suggests an origin linked to subduction (Thompson et al., 1984; among others). This is in agreement with the geotectonic setting discrimination diagrams of Pearce et al. (1984) (Y + Nb vs. Rb, Y vs. Nb), and the Th/Nb vs SiO_2 and La/Nb vs SiO_2 diagrams of Müntener et al. (2018) indicating a subduction setting (Fig. 8e,f and g). Regarding cortical thickness estimations, the La/Yb(N) ratio (5.15–10.75) (normalized to chondrite, Nakamura (1974)), indicates a range between 18 and 23 km according to Hu et al. (2017) ($Dm = 27.78 \ln[0.34 (La/Yb)N]$) (Fig. 8h), suggesting

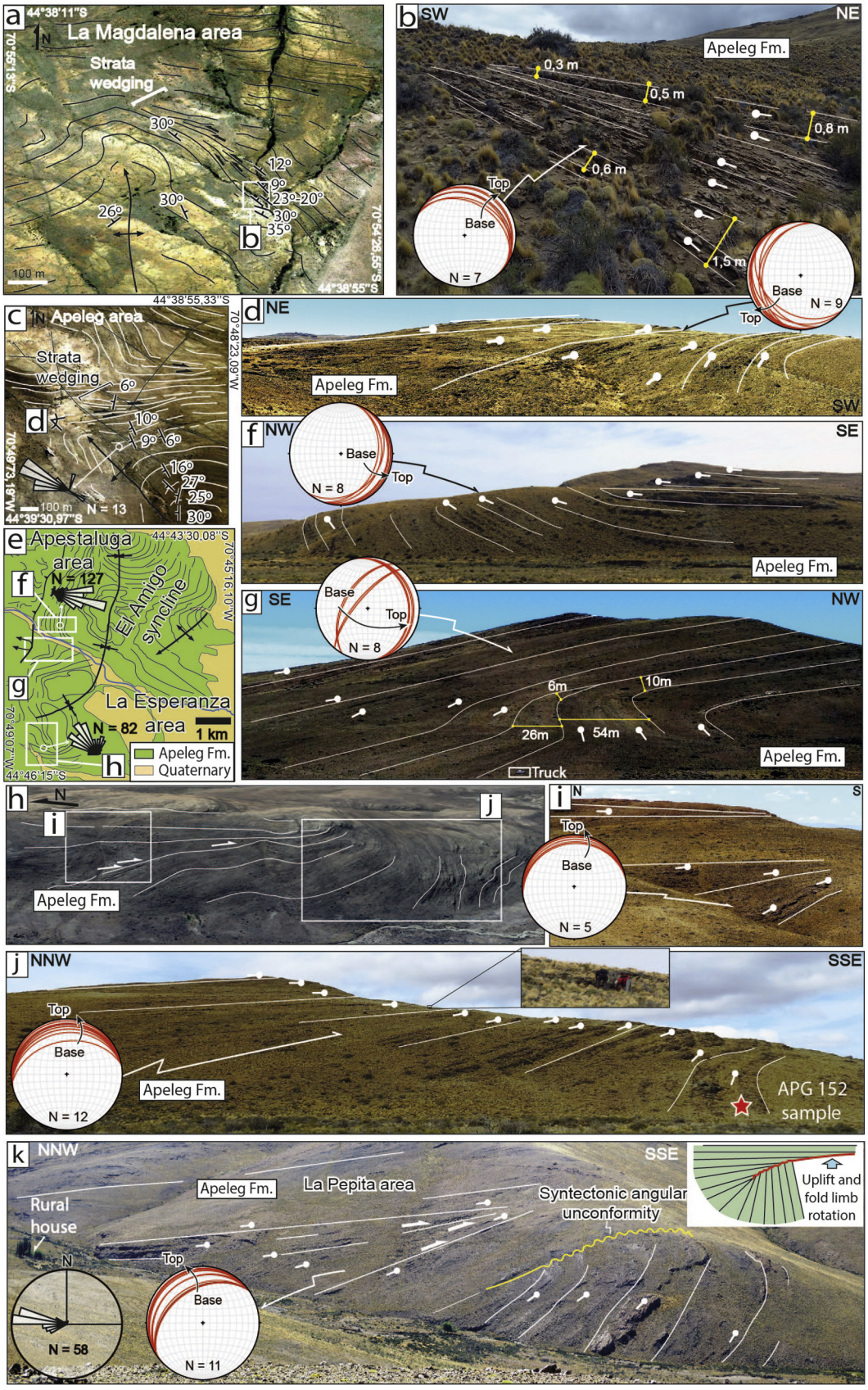

Fig. 5. Syncontractional growth strata from the Apeleg Formation. a) Map view of growth strata at the La Magdalena area. b) field data of the basal section of growth strata in the later area. c) *Landsat* image showing structural data, paleocurrent results, and d) a field picture of growth strata at the Apeleg area. e) Local sketch map of the Apestaluga-La Esperanza areas showing structural data, paleocurrent results, and locations of growth structures related to the El Amigo syncline. f) Growth strata in the northern sector of the Apestaluga area and g) anticline with overturned fanning strata to the south. h) *Google Earth* image showing the location of (i and j) growth structures in the La Esperanza area. k) Paleocurrent data and growth strata at La Pepita area. For locations see Fig. 2c. Original field photograph can be found at supplementary information in Fig. S1.

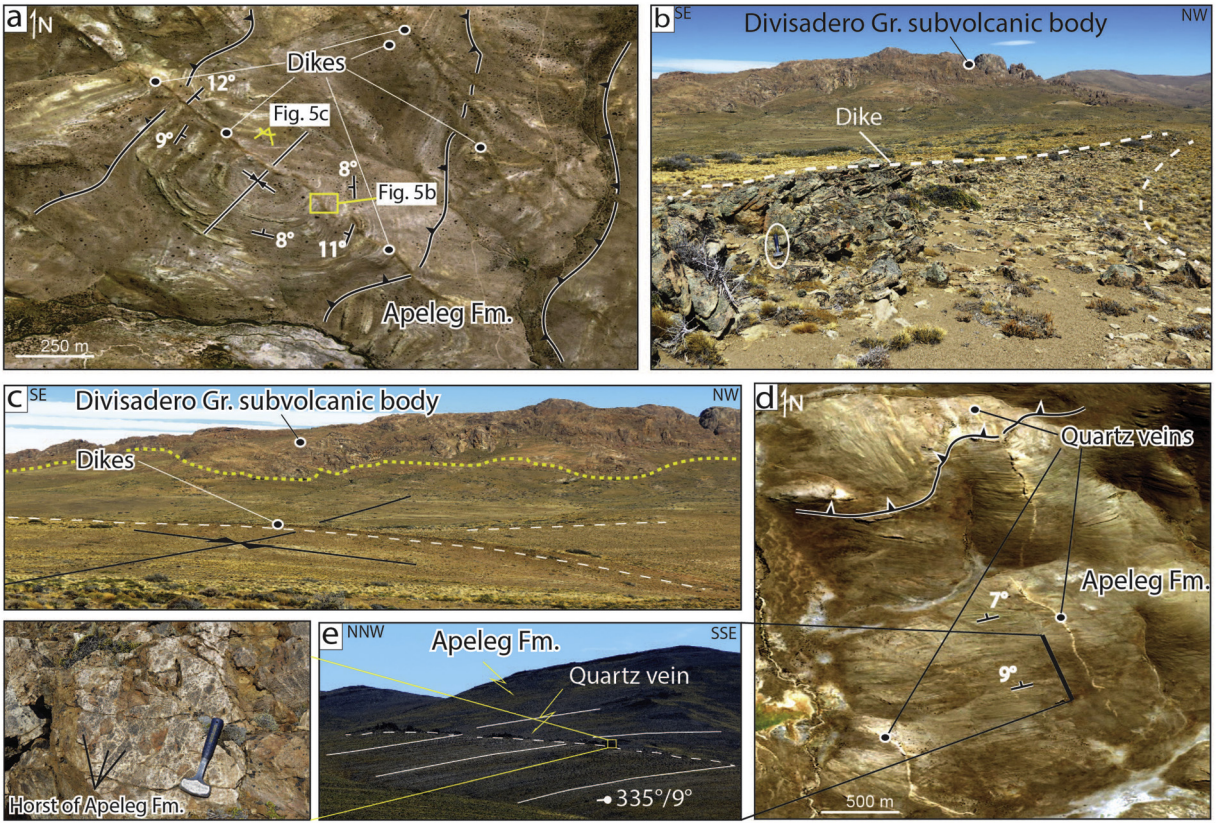

Fig. 6. Cross-cutting structural evidences of the late Early Cretaceous contraction in the external area of the LPF. (a) *Landsat* image and (b–c) field pictures showing contractional structures cut by rhyolitic dikes related to the Aptian Divisadero Group volcanic rocks in the Apestaluga area. (d) *Landsat* image and (e) field picture showing a thrust cut by quartz veins related to the Divisadero Group magmatism in the La Pepita area. See Fig. 2c for the location.

the existence of a thin Early Cretaceous crust. This is also evidenced by the low values of Sm/Yb ratio (1.14–2.41) indicating magma generation at relatively low pressure in the stability range of pyroxene (Fig. 8i. Kay et al., 1991).

Crustal thickness estimation derived from 117 to 107 Myr rocks of the Divisadero Group indicates that initial Andean contraction recorded in the study area took place in a thin crust. A reasonable explanation for this has been recently provided by Echaurren et al. (2017) based on a regional analysis of the Divisadero Group magmatism. These authors suggested that a thin crust at the onset of Andean shortening was a feature inherited from the previous Late Jurassic-earliest Cretaceous extensional stage associated with the opening of the ARB (Fig. 2b).

Table 3
Classifications for sandstone petrographic point counts.

Symbol	Description
Qm	Monocrystalline quartz with flash extinction
Qm-ond	Monocrystalline quartz with ondulant extinction
Qpg	Polycrystalline quartz
Ko	K-feldspar (orthose/orthoclase)
Kper	K-feldspar (perthite)
Km	K-feldspar (microcline)
P	Plagioclase feldspar
Gl	Glauconite
LVA-fels	Acid volcanic fragments with felsitic texture
LVA-silicif	Acid volcanic fragments with evidence of silicification
LVI	Intermediate volcanic fragments
Pyro	Pyroclastic fragments
M	Mica fragments
LS	Sedimentary fragments
Q-LVA	Quartz crystals within acid volcanic fragments
P-LVA	Plagioclase feldspar crystals within acid volcanic fragments
K-LVA	K-feldspar crystals within acid volcanic fragments
K-LPlut	K-feldspar crystals within granitic/plutonic fragments
Q-LPlut	Quartz crystals within granitic/plutonic fragments
Gar	Garnet
Q	Total quartz (Qm + Qm-ond + Qpg + Q-LVA + Q-LPlut)
F	Total feldspar (Ko + Kper+Km + P + P-LVA + K-LVA + KLPlut)
L	Total Lithic fragments
Lt	Total Lithic fragments with Qpg

5. Discussion

5.1. Tectonic setting of the Apeleg Formation

Sedimentological data presented in Section 3 indicates that deposition associated with the Apeleg Formation was marked by the accumulation of ~100–350 m of sediments in a deltaic environment (Fig. 3). Additionally, structural data described in section 4 shows for the first time that these deposits represent multiple lines of evidence for growth strata and progressive unconformities directly related to the development of contractional structures (Fig. 5). The contraction in the study area is further corroborated by the presence of folds and thrusts affecting the Apeleg Formation that are intruded by relatively undeformed rhyolitic dikes and quartz veins related to the Aptian-Albian Divisadero Group magmatism (Fig. 6). As a whole, our tectosedimentary analysis indicates a synorogenic origin for the Apeleg Formation, which contrasts most recent proposals claiming deposition linked to a thermal subsidence mechanism (González-Bonorino and Suárez, 1995; Bell and Súarez, 1997; Depine and Ramos, 2004; Demant and González, 2010; Suárez et al., 2009b). We suggest that growth-strata in the study area could be the result of wedge-top depozone dynamics in a foreland basin system (DeCelles, 2012). In these settings, the active orogenic front is often buried and growth geometries develop due to simultaneous sedimentation and deformation. However, the scarcity of published data in the subsurface area of the ARB does not allow at the moment inferring more details about the characteristics of the rest of

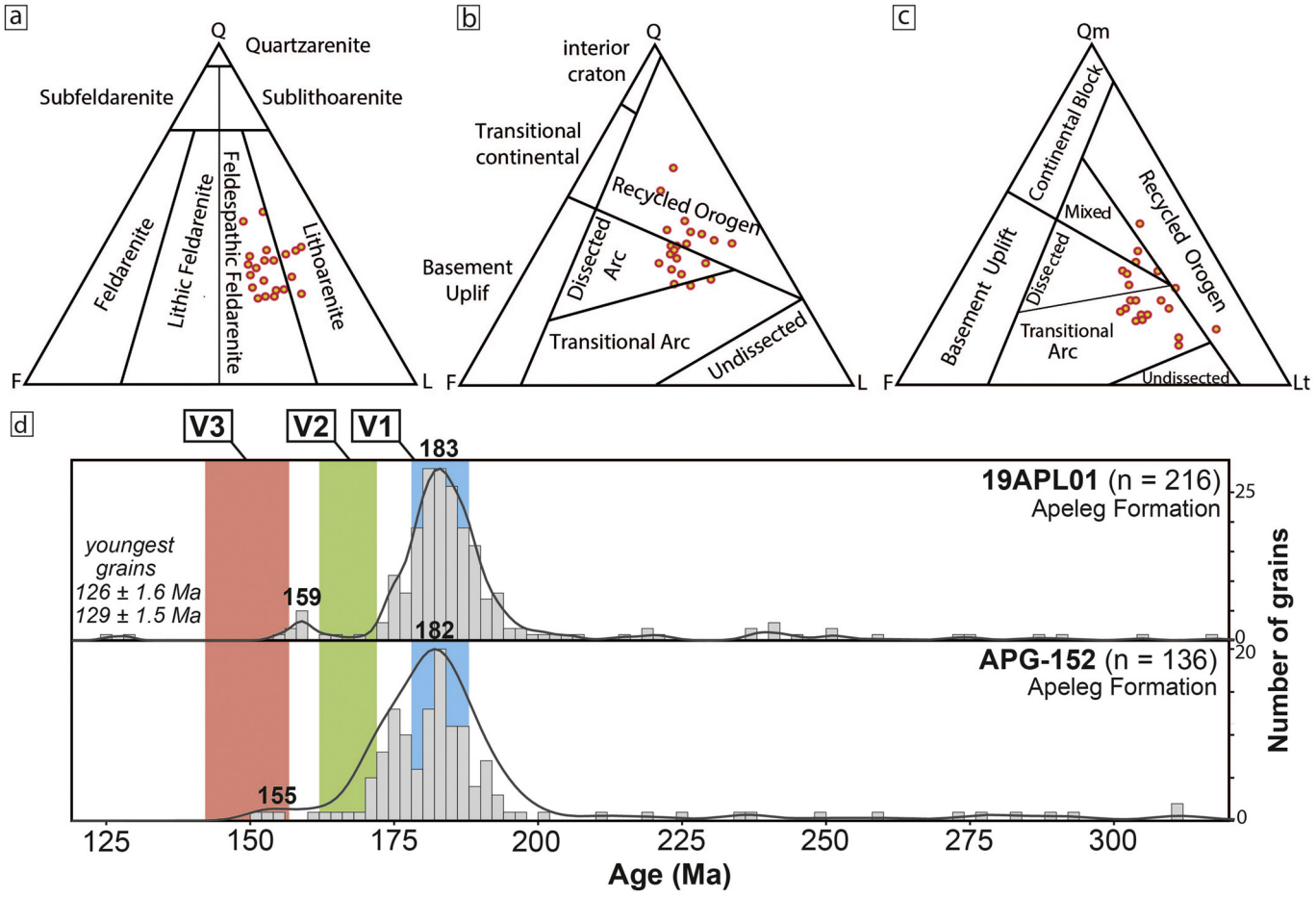

Fig. 7. a) Quartz-feldspar-lithic (QFL) sandstone nomenclature (Folk et al., 1970). b) QFL tectonic provenance (Dickinson, 1983). c) QmFLt tectonic provenance (Dickinson, 1983). d) Probability density plots and histograms of U-Pb detrital zircon ages.

the potential depozones. Alternatively, the Apeleg Formation could have form part of an incipient broken foreland basin system (Strecker et al., 2011) whose maximum expression took place in late Early to Late Cretaceous during deposition of the Chubut Group to the east of the study area (Gianni et al., 205). In any case, the Apeleg Formation indicates the inception of shortening and incipient activity of the North Patagonian orogenic front in latest Hauterivian/Barremian to Aptian times (~130 to 122 Myr). Estimation of crustal thickness from geochemical data of ~117–107 Myr igneous rocks of the Divisadero Group intruding folded rocks of the Apeleg Formation indicates that initial shortening took place in a thin crust (Fig. 8). Such conditions were most likely inherited from previous Late Jurassic-earliest Cretaceous backarc rifting stage in the ARB (Echaurren et al., 2017). A similar case has been recently reported in the early evolution of the southern Tibetan plateau, where a thin continental crust, probably at or below sea level, existed during early Tertiary time prior to and during the early stages of collision of India (DePaolo et al., 2019).

It is worth noting that the marine regression associated with the Apeleg Formation took place in a context of increasing global sea level (Haq et al., 1987; Hallam and Cohen, 1989; EXXON Petroleum Company, 1988; Vérard et al., 2015) (Fig. 1b). This observation strengthens the idea of a forced origin for the regression (Aguirre-Urreta and Ramos, 1981), as also inferred from data indicating coeval contractional activity presented in this study.

Further insights into this basin stage are provided by provenance results presented in Section 5. In provenance studies the initiation of orogeny and foreland basin development are commonly interpreted based on marked shifts on sediment sources, often determined through U/Pb detrital zircon geochronology and/or sandstone-conglomerate composition (e.g. Horton, 2018a). In the Andes, this change has been frequently associated with the detection of arc and basement sources from the western active margin. This is interpreted as indicating the establishment of an orogenic drainage divide (e.g. Di Giulio et al., 2016; Horton, 2018a for a synthesis). Notably, despite evidence indicating contraction during deposition of the Apeleg Formation, provenance data does not suggest the existence of a well-defined drainage divide during this basin stage. In this regard, data obtained from conglomerate clasts counts (high silicic volcanic clasts proportions; Fig. 3), sandstone petrography (high proportions of silicic volcanic lithic Fig. 7d), and detrital zircon U-Pb geochronology (conspicuous <183 and 176 Ma age peaks; Fig. 7d) indicate a dominant eastern sediment source in the Patagonian interior with minor contributions from the western margin (smaller age population between ~160–150 Ma; Fig. 7d).

We suggest that this could be the potential outcome of a primitive mountain-building stage represented by the Apeleg Formation. In this regard, we suggest that the low shortening magnitude of this early stage would have been insufficient to develop a noticeable sediment source in the active margin and hence, a well-defined drainage divide (Fig. 9). Topographic build-up would have been further delayed by the existence of an attenuated crust in the ARB previous to initial shortening (Echaurren et al., 2017). Further insights can be provided from the analysis of the documented growth strata. As seen in Fig. 5, most growth geometries are related to folds where steeply tilted lower strata are covered to the top by gently dipping (10–5°) beds. The presence of these geometries is typical of growth strata reflecting structure uplift rates below sedimentation rates (Burbank et al., 1996) precluding

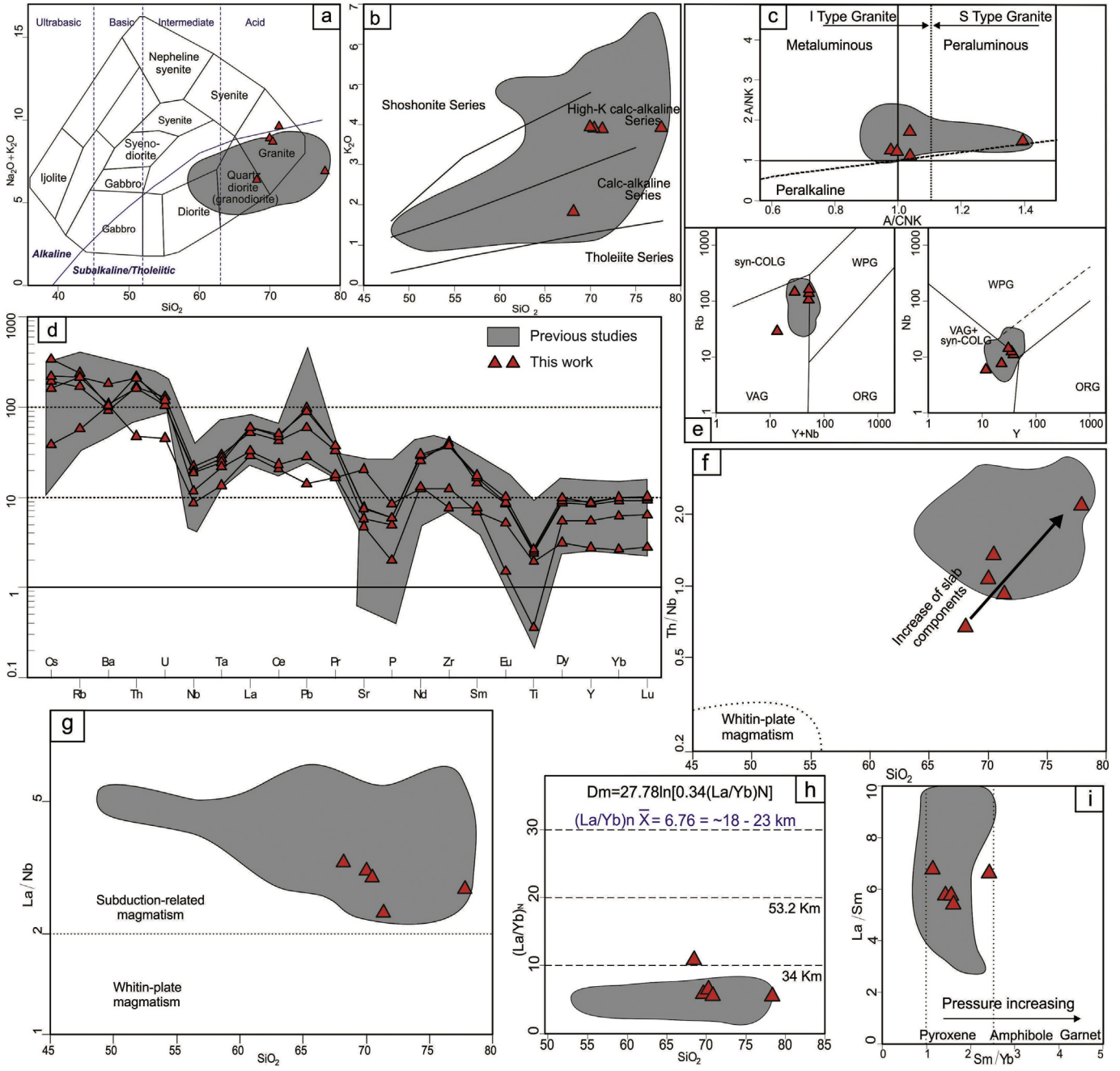

Fig. 8. a) TAS diagram (Cox et al., 1979). b) K_2O vs. SiO_2 diagram (Peccerillo and Taylor, 1976). c) A/CNK vs. A/NK diagram (Shand, 1943). Field of I- and S-type granites of Chappel and White (2001). d) Trace multielemental diagram normalized to primitive mantle (McDonough and Sun, 1995). e) Geotectonic setting discrimination diagrams of Pearce et al. (1984). f) Th/Nb vs SiO_2 diagram after Müntener et al. (2018). g) La/Nb vs SiO_2 diagram after Müntener et al. (2018). h) SiO_2 vs La/Yb(N), crustal thickness estimations from Hu et al. (2017). i) Light rare earth elements (Sm/Yb) vs. heavy rare earth elements (La/Sm) diagram. Light blue area in all diagrams represents data compilation from Echaurren et al. (2017) of Divisadero Group in the North Patagonian Andes. See Fig. 2c for sample location. (For interpretation of the references to color in this figure legend, the reader is referred to the web version of this article.)

basement exposure and the development of local basin sources. From a broader perspective, low topography at this stage is evident from the sedimentary environments in the Apeleg Formation indicating deposition close to sea level (Fig. 3) and the shallow marine nature of this unit to the southwest of the ARB (Bell and Súarez, 1997). The latter indicates that significant crustal thickening and related isostatic topography was not established at that time. This is confirmed by our estimations based on La/Yb ratios indicating an attenuated crust (~20–18 km) at the time of rhyolitic dikes emplacement after incipient shortening in the study area (Fig. 8e and f). Thus, during this stage, the ARB would have been dominated by sources from the Patagonian foreland delivered by deltaic systems. In these, sediments may have bypassed incipiently growing low-amplitude structures in the ARB, similarly to those documented by López-Blanco et al. (2003) in the South-Pyrenean foreland basin. In this context, rivers would have transported materials eroded from intraplate highs to the east (Fig. 9). In the hypothetical context of a foreland basin system for the Apeleg Formation, the latter sources could have been linked to incipient forebulge uplift (Horton et al., 2010). On the other hand, in the case of an incipient broken foreland basin system, this source could have been associated with subtle intraplate deformation (e.g. Ghiglione et al., 2015; Hurtado et al., 2018).

Therefore, the existence of a thin crust at the onset of shortening, sedimentary environments suggesting deposition close to sea level,

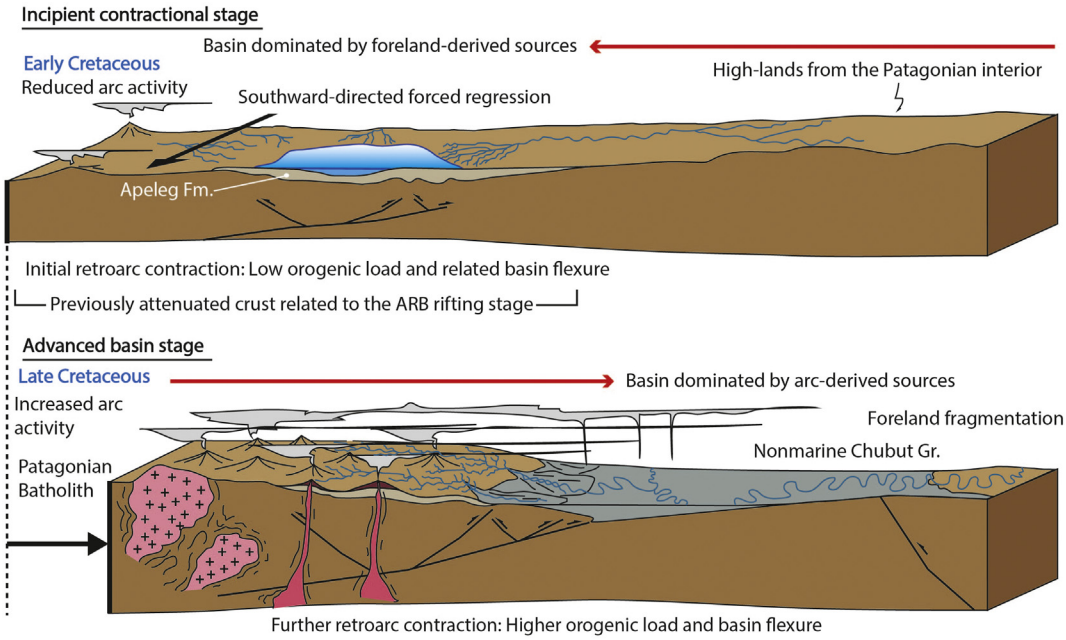

Fig. 9. Conceptual model for the tectonic setting of the Apeleg Formation in the ARB. Incipient contractional basin stage: Inception of initial shortening in an attenuated crust in Early Cretaceous times produced a progressive forced marine regression during deposition of the Apeleg Formation. During this stage, Andean topography was negligible, orogenic load and related basin subsidence was low, and arc activity was reduced. Hence, basin sediments were mostly supplied from the relatively higher foreland area by west-directed fluvial-deltaic systems. Advanced basin stage: In Late Cretaceous times, vigorous arc activity and further shortening and orogenic load, favored the establishment of a dominant active margin source in the west deriving nonmarine synorogenic sediments to the east (Chubut Group).

growth strata geometries linked to structures not exposing the basement and foreland-derived provenance are not in conflict. All these indicate that at the onset of contraction, a high topography (Andes) with a clear drainage divide was not developed immediately, as expected in the early stages of mountain building.

A similar case was recently documented in the northern sector of the Austral basin. There, provenance studies in indicate that Aptian-Albian successions were derived from the Patagonian continental interior and it was interpreted as the result of intraplate deformation (Ghiglione et al., 2015). However, most recent studies in these same successions based on the anomaly of magnetic susceptibility (AMS) indicate that E-W contraction took place during deposition of these units (Ramos et al., 2016; Aramendía et al., 2018). Thus, the Aptian-Albian depocenters of the northern Austral basin were linked to the initial stage of Andean growth at those latitudes despite not presenting a clear Andean zircon provenance (Aramendía et al., 2018; Ronda et al., 2019).

A western active source and a more mature drainage divide began to develop in the Late Cretaceous recognized through in provenance analysis of the nonmarine Chubut Group and the marine Paso del Sapo and Lefipán Formations in the foreland area (Tunik et al., 2004; Butler et al., 2019) (Fig. 9). In this regard, recent paleoaltimetry studies by Colwyn et al. (2017) indicate that the Patagonian orogenic rain shadow was already established by ~62 Ma. According to these authors, the North Patagonian Andes would have been a long-lived topographic feature, mostly built during the Late Cretaceous-Paleocene orogenic phase.

Therefore, we suggest that the synorogenic deposition of the Apeleg Formation constitutes a primitive contractional basin stage. The latter would have developed before significant orogenic load, lithospheric flexure and basin subsidence (Fig. 9).

5.2. Synthesis of post-Gondwanic initial contraction along the Andean orogen and implications for geodynamic models of subduction orogeny

In order to place Early Cretaceous contraction in the ARB in the context of the Andean evolution, here we summarize studies documenting the earliest orogenic stages along-strike this mountain belt.

The early evolution of the Northern Andes (~10°N to 0°) is considered a classic accretionary orogeny associated with active subduction since Jurassic times (Restrepo and Toussaint, 1991; Ramos, 2009) (Fig. 1a). Two end-member models have been suggested to explain the Cretaceous tectonic evolution of this orogenic sector. One proposing contraction related to accretion of one or more oceanic terranes since Early Cretaceous times (e.g. Villagómez and Spikings, 2013; Spikings et al., 2015) and the other suggesting the existence of an Early Cretaceous extensional continental arc associated with an oceanic floored backarc basin. The latter would have formed between ~141 and 100 Myr and was accreted in latest Cretaceous (Kennan and Pindell, 2009; Nivia et al., 2006; Spikings et al., 2015; Villagómez et al., 2011). This hypothesis is compatible with the preserved mantle velocity structure in that region that can only be reconstructed through numerical modeling when considering the existence of an intraoceanic subduction and an oceanic back-arc basin (Braz et al., 2018). The Late Cretaceous contraction has been suggested based on the distribution and composition of sedimentary rocks, detrital thermochronology, and geochronology of igneous complexes that indicate that the active margin shifted to contraction around 115 Ma (Villagómez et al., 2011; Spikings et al., 2015). Nevertheless, according to a recent study of Zapata et al. (2019), back-arc basin extension would have continued up to 100 Ma based on the documentation of an active arc at that time and the *syn*-extensional nature of the basin infill. Independent data supporting initial contraction of the Northern Andes at 100 Ma is also provided by the recent plate reconstructions of Braz et al. (2018) that incorporate the velocity mantle structure into geodynamic numerical models.

The Central Cordillera of Colombia and the Eastern Cordillera of Ecuador began to experience more significant shortening from Maastrichtian to early Paleocene times (Cooper et al., 1995; Barragán, 1999; Aleman and Ramos, 2000; Ruiz, 2002; Baby et al., 2004; Gómez et al., 2003, 2005; Vallejo, 2007; Horton et al., 2010; Mora et al., 2010; Villagómez and Spikings, 2013; Reyes-Harker et al., 2015). The latter is confirmed by the basin deposition that depicts a sudden increase in accumulation rates between ~70 and 60 Myr associated with the foreland flexure subsidence (Horton, 2018a).

In the northern Central Andes between 0° and 18°S, initial orogeny is marked by synorogenic deposition and the development of angular unconformities during the Late Cretaceous Mochica and Peruvian phases at ~100 Ma and ~90–70 Myr, respectively (Steinmann, 1929; Mégard, 1984; Jaillard et al., 2000; Pfiffner and Gonzalez, 2013) (Fig. 1a). Orogenic load related to the Mochica tectonic phase allowed the development of the Turonian-Maastrichtian Andean Basin, a foreland basin system encompassing northern Peru to south Bolivia including the Potosí, Marañon, Acre and Oriente basins (Reyes, 1972; Sempere, 1995; Jaillard and Soler, 1996; Sempere et al., 1997; Jaillard et al., 2000; Menegazzo et al., 2016) (Fig. 1a).

Further to the south in the Central Andes between 20°S and 25°S, the beginning of Cretaceous contraction is well recorded within the Tarapacá and Atacama foreland basins (Schiller, 1912; Mpodozis et al., 2005; Arriagada et al., 2006; Fuentes et al., 2018; Martínez et al., 2018a) (Fig. 1a). The oldest synorogenic deposits have been described in the Atacama basin and belong to the Tonel Formation with a maximum depositional age of ~107 Ma (Bascuñán et al., 2016).

In the Southern Central Andes between 26° and 33°S, structural evidence and dating of synorogenic strata indicate an initial growth stage between ~105 and 80 Myr (Boyce et al., 2014; Martínez et al., 2015, 2018b). The best exposures of the Cretaceous foreland basin deposits in the Southern Central Andes are preserved in the Neuquén basin (32°30′-40°S) (Fig. 1a). In this area, timing of foreland basin inception is either interpreted to correspond with the base of the nonmarine Neuquén Group and Diamante Formation (~107–98 Myr) (Groeber, 1946, 1947; Ramos, 1981b; Tunik et al., 2010; Di Giulio et al., 2012; Fennell et al., 2015; Balgord and Carrapa, 2016; Gómez et al., 2019) or an the unconformity between the Huitrín Formation and the Rayoso Group (Cobbold and Rossello, 2003; Mosquera and Ramos, 2006), at sometime after 124 Ma and before ~120 Myr.

In the North Patagonian Andes between 40° and 46°30′S the early Andean growth is mostly inferred based on the finding of a late Aptian angular unconformity separating the Apeleg Formation from the Divisadero Group and spanning the 118–121 Myr time interval (Ramos, 1981a; Folguera and Iannizzotto, 2004; Suárez et al., 2009b; Orts et al., 2012; Echaurren et al., 2017) (Fig. 2b). This stage has also been inferred based description of synorogenic deposition linked to intraplate deformation dated between ~115–65 Myr (Gianni et al., 2015, 2018a, 2018b; Echaurren et al., 2017).

The Cretaceous contraction in the Southern Andes (Austral Patagonian and Fuegian Andes) between 46°30′S and 56°S is well established based on structural evidence, metamorphic events, thermochronology and by the conspicuous formation of the Austral-Magallanes foreland basin (Dalziel et al., 1974; Dalziel, 1981, 1986; Bruhn and Dalziel, 1977; Nelson et al., 1980; Kohn et al., 1995) (Figs. 1a and 2a). In this area, the earliest deformation is related to the closure of the oceanic floored Rocas Verdes basin (Dalziel et al., 1974). This extensional basin formed through northward unzipping of the backarc area from Early to Late Jurassic times (e.g. Malkowski et al., 2016) (Fig. 2a). According to Calderon et al. (2013), the beginning of ophiolite obduction began between 120 and 110 Myr and terminated before ~80 Ma giving place to the Austral-Magallanes foreland basin. In the northern sector of this basin, between 46°S and 49°S, Aguirre-Urreta and Ramos (1981) suggested that a proto-Patagonian Cordillera was first uplifted in Aptian-Albian times. Regressive deposits associated with this stage and dated between 122 and 110 Myr have been interpreted whether as the synorogenic deposits linked to Patagonian Andes growth (Aguirre-Urreta and Ramos, 1981) or intraplate deformation linked to South Atlantic opening (Ghiglione et al., 2015). The former hypothesis has been recently favored based on the anomaly of magnetic susceptibility indicating E-W contraction during deposition of this unit related to the Andean fold-thrust belt propagation at this time (Aramendía et al., 2018). In the southern Austral-Magallanes basin synorogenic deposition began around 112–110 Myr at 49°-50°S and propagated southward up to ~89–85 Myr in the Fuegian Andes (Wilson, 1991; Fildani and Hessler, 2005; McAtamney et al., 2011; Ghiglione et al., 2014; Malkowski et al., 2015; among many others).

Sediment accumulation curves from the Austral-Magallanes basin suggest accelerated flexure-related deposition began at ~100 Ma and persisted until ~60 Ma (Biddle et al., 1986; Horton, 2018a). The diachronic foreland basin deposition has been explained by the southward propagation of backarc closure of the preexisting Rocas Verdes basin (e.g. Malkowski et al., 2016; Ghiglione et al., 2016; Ronda et al., 2019).

The synthesis above indicates that most of the Andean margin records a generalized growth stage mainly between ~110 and 90 Myr (Cobbold et al., 2007; Somoza and Zaffarana, 2008). However, evidence of the initial contractional deformation at 122–118 Myr is found in a discrete sector between 40° and 47°S in the North Patagonian Andes and the Northern sector of the Austral Patagonian Andes. We note that synorogenic deposits of the Apeleg Formation (~130–122 Myr) not only constitute the oldest sedimentary record of Early Cretaceous contraction in this 42°-47°S segment, but most likely of the entire Andean Cordillera. Hence, the ARB preserves a unique record of the earliest evolutionary stage of the Andes.

A striking feature resulting from this synthesis is that the beginning of Andean evolution seems to have been characterized by a diachronic tectonic uplift pattern (Fig. 10). We note that besides the Rocas Verdes-Austral basins segment of the southern Patagonian Andes (~950 km) that experienced a southward growth, the rest of the Andes (~6500 km) depict a northward propagating tectonic uplift pattern (Fig. 10).

As described in the synthesis above the earliest margin contraction is recorded in the segment from 42° to 47°S to the south at 122–118 Myr and locally earlier at ~130–124 Myr considering sedimentation of the lower section of the Apeleg Formation in the ARB (Fig. 10). The segment affected by early contraction could be extended up to 52°S if we consider the beginning of the Rocas Verdes ophiolite obduction at 120–110 Myr as suggested by Calderon et al. (2013). At this time, the rest of the Andean margin was experiencing thermal subsidence and/or intraarc to backarc extension (e.g. Jaillard and Soler, 1996; Charrier et al., 2007; Zapata et al. 2019). At around, 100–90 Myr contractional deformation propagated to the north and affected the entire Andean margin (Fig. 10). Although delayed in time respect to our revision, Horton (2018a) described a contemporaneous shift in accumulation and sedimentary polarity first in the southern Andes at ~100 Ma, and then at ~70–60 Myr in the rest of the Andean orogen. We suggest that this tectonic pattern is not likely the result of selective erosion of earliest synorogenic deposits in the Andes. The latter is supported by the preservation of Early Cretaceous sedimentary rocks in several basins of the Central and Northern Andes associated with thermal subsidence or basin extension (Jaillard and Soler, 1996; Charrier et al., 2007; Ramos, 2009; Menegazzo et al., 2016; Fuentes et al., 2018; Zapata et al. 2019; among others).

The potential diachronous character of the Andean birth has major implications for the driving mechanism behind initial orogeny, an issue intensely debated (Somoza and Zaffarana, 2008; Schellart, 2017; Faccenna et al., 2017; Chen et al., 2019). It has been suggested that this stage does not correlate with the dynamics of the Atlantic Ocean as initially thought and that early Andean deformation lagged several millions of years after the ocean opening (e.g. Oncken et al., 2006; Barnes and Elhers, 2009; Faccenna et al., 2017). However, although the strongest deformation and orocline formation in the Central Andes is Cenozoic in age, as reviewed above, contraction can be tracked back up to Cretaceous times along strike the Andean Cordillera (see also Ramos, 2009; Horton et al., 2018).

From our updated synthesis we note that the diachronic inception of Andean orogeny mimics roughly the evolution of the Atlantic Ocean opening (Fig. 10). In this regard, the earliest contraction and synorogenic deposition appeared in the Patagonian Andes after emplacement of the first oceanic crust (134–132 Myr; Nürnberg and Müller, 1991) in the southernmost part of the South Atlantic Ocean and more evidently during South Atlantic rifting acceleration at

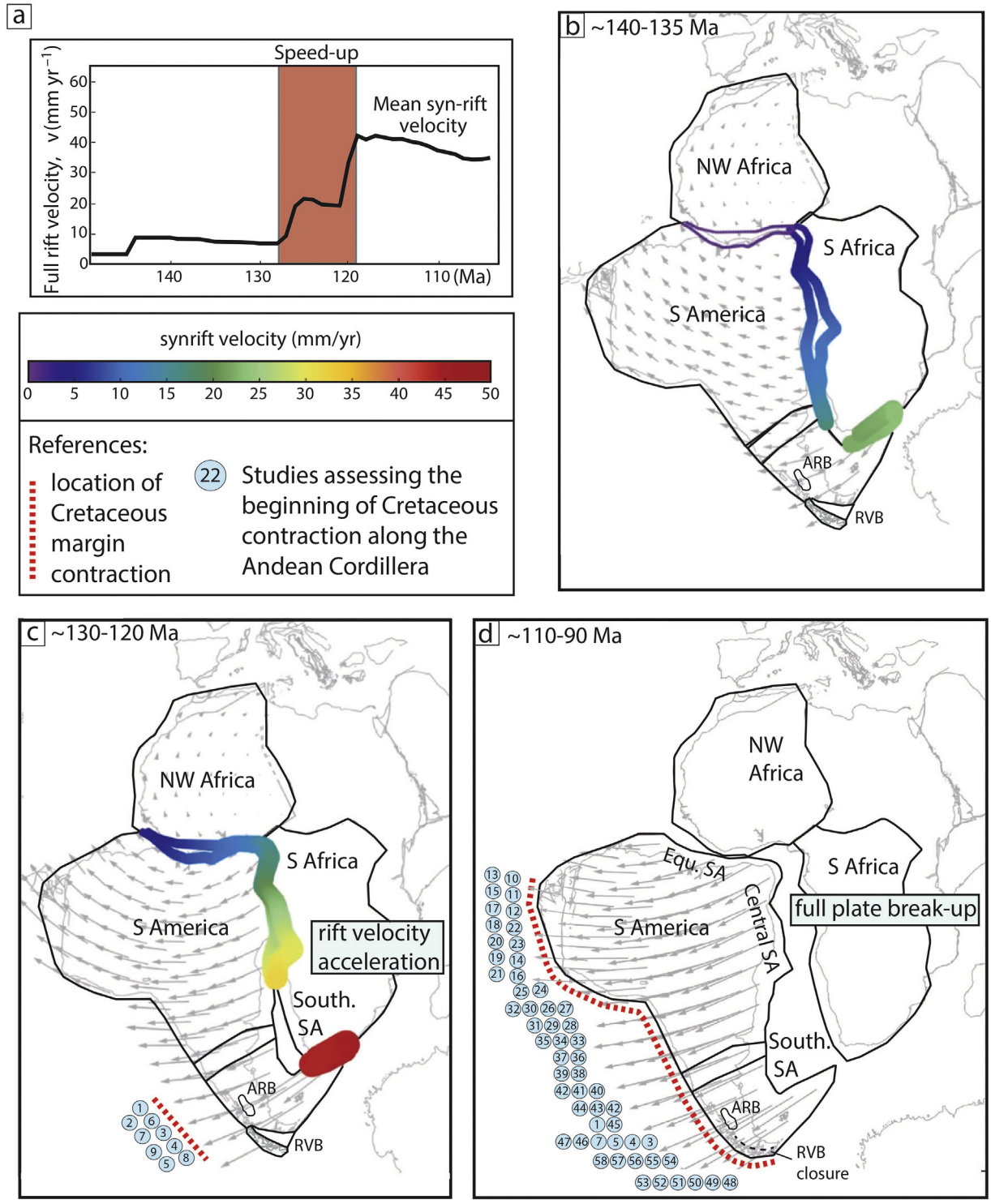

Fig. 10. a) Atlantic synrift modified from Brune et al. (2016) showing an acceleration in rifting velocity between ~130 and ~120 Myr (b-d). Conceptual model linking northward propagating South Atlantic opening and upper plate drift to the diachronic Andean birth. Reconstruction indicating rift velocity (coloured areas) and continent motion (Africa fixed) is modified from Brune et al. (2016). Main works describing post-Gondwanic initial Andean contraction in Cretaceous times are: 1) Cobbold and Rossello (2003), 2) Mosquera and Ramos (2006), 3) Ramos (1981a), 4) Folguera and Iannizzoto (2003), 5) Suárez et al. (2009a), 6) Orts et al. (2012), 7) Echaurren et al. (2016, 2017), 8) Aramendía et al. (2018), 9) This sudy, 10) Pindell and Kennan (2009), 11) Villagómez et al. (2011), 12) Spikings et al. (2015), 13) Cooper et al. (1995), 14) Barragán (1999), 15) Aleman and Ramos (2000), 16) Ruiz (2002), 17) Baby et al. (2004), 18) Gómez et al. (2003, 2005), 19) Vallejo (2007), 20) Horton et al. (2010), 21) Mora et al. (2010), 22) Villagómez and Spikings (2013), 23) Reyes-Harker et al. (2015), 24) Steinmann (1929), 25) Mégard (1984), 26) Jaillard et al. (2000), 27) Pfiffner and González (2013), 28) Réyes (1972), 29) Sempere (1995), 30) Jaillard and Soler (1996), 31) Sempere et al. (1997), 32) Menegazzo et al. (2016), 33) Mpodozis et al. (2005), 34) Arriagada et al. (2006), 35) Fuentes et al. (2018), 36) Martínez et al. (2018a), 37) Bascuñan et al. (2016), 38) Boyce et al. (2014), 39) Martínez et al. (2015; 2018b), 40) Groeber (1946), 41) Ramos (1981b), 42) Tunik et al. (2010), 43) Di Giulio et al. (2012), 44) Fennell et al. (2015), 45) Balgord and Carrapa (2016), 46) Gianni et al. (2015, 2018a), 47) Suárez and De la Cruz (2001), 48) Dalziel 1974, 49) Dalziel (1981, 1986), 50) Bruhn and Dalziel (1977), 51) Nelson et al. (1980), 52) Kohn et al. (1995), 53) Wilson (1991), 54) Fildani and Hessler (2005), 55) McAtamney et al. (2011), 56) Ghiglione et al. (2014), 57) Malkowski et al. (2015), 58) Ronda et al. (2019). Abbreviations are; ARB: Aysén-Río Mayo Basin; RVB: Rocas Verdes Basin; Central SA, Central South Atlantic; Equ. SA, equatorial South Atlantic; SA, southern South Atlantic; NW Africa, Northwest Africa; S Africa, South Africa; S America, South America. Figure modified from Brune et al. (2016). See text for further details.

~122–120 Ma likely (Heine and Brune, 2014; Brune et al., 2016) (Fig. 10). Plate margin contraction at this time resulted from the onset of upper-plate motion overcoming trench retreat as suggested for more recent Andes stages (e.g. Oncken et al., 2006; Somoza and Zaffarana, 2008). This abrupt increase in upper-plate motion was explained by Brune et al. (2016) through numerical modeling. These authors attributed this process to a shift from a slow- rift to a fast-rift stage triggered by sudden thermomechanical weakening during plate breakup. As seen in the study of Brune et al. (2016), this abrupt upper-plate acceleration stage was fastest in the South Atlantic Ocean, which explains the oldest evidence of Andean margin contraction at those latitudes (Fig. 10). Also, this process would have also played a key role in is triggering a modification in the subduction angle in southern South America at that time (Gianni et al., 2018b). It is worth noting that at this stage the progressive closure of the Rocas Verdes backarc basin and subsequent arc-continent collision may have delayed early deformation in southernmost South America (Fuegian Andes) respect to the Patagonian Andes to the north. Subsequently, early contractional deformation propagated northward achieving its climax between ~100 and 90 Myr during the full continental breakup and further westward drifting of South America (Somoza and Zaffarana, 2008; Husson et al., 2012; Heine and Brune, 2014) (Fig. 10). This northward younging of orogen development is not accounted for the numerical modeling of Andean mountain-building of Capitanio et al. (2011) and Faccenna et al. (2017). These models reproduce the critical shift from backarc extension to contraction at ~70 Ma or later (see Fig. 3b in Schellart, 2017), which is in stark contrast with the updated Andean synthesis and the results presented in this study.

High resolution numerical modeling of Schellart (2017) considering the influence of deep mantle subduction on continental trenchward motion reproduces effectively the initial timming of contraction at ~125, but also fails to reproduce the northward propagating pattern of Andean growth. This study predicts that backarc extension changes to shortening in the Central Andes at ~120 Ma, while extension continues periodically until 80–120 Myr away from the centre (Fig. 3b). The latter would produce an overall outward growth pattern from the Central Andes which is inconsistent with the geological observations reviewed above.

Hence, although lower mantle slab penetration, subduction length, and slab age may have significantly shaped late orogenic evolution, these processes are not responsible for the establishment of the initial tectonic shift from an extensional subduction setting to a contractional subduction zone (i.e. Chilean-type margin, Uyeda and Kanamori, 1979). Instead, the close relation to Atlantic Ocean dynamics and related upper plate drift suggest a dominant role for this process at least at the beginning of Andean orogeny (Dalziel et al., 1974; Baker et al., 1981; Mpodozis and Ramos, 1990; Coney and Evenchick, 1994, Heuret and Lallemand, 2005; Husson et al., 2012; Yang et al., 2019). At this moment a northward propagating mantle drag at the base of the lithosphere associated with the progressive development of the Atlantic Ocean convection cell (Husson et al., 2012), would have produced a diachronic drifting of South America. This process resulted in a northward-younging overriding of the Pacific trench overcoming slab roll-back and triggering the diachronic tectonic uplift pattern observed during the Andean birth stage (Fig. 10). Subsequently, in Paleogene to Neogene times, further changes in several geodynamic parameters such as upper-plate velocity (Silver et al., 1998), slab age, subduction length and depth (e.g. Capitanio et al., 2011; Faccenna et al., 2017; Schellart, 2017; Chen et al., 2019) as well as the onset of critical climatic conditions (e.g. Lamb and Davis, 2003; Armijo et al., 2015) would have significantly enhanced orogen contraction, profoundly shaping the Andean orogen to achieve its current state. The joint action of these processes would have resulted in the present Cordillera morphology associated with the development of along-strike orogen symmetry, large-scale rotations linked to the Bolivian Orocline and orogenic plateau formation in the Central Andes (e.g., Oncken et al., 2006; Armijo et al., 2015).

6. Conclusions

A multidisciplinary approach demonstrates a synorogenic origin for the Apeleg Formation corresponding to the first concrete report of latest Hauterivian/Barremian to Aptian (~130–122 Myr) syntectonic deposition related to the initial growth of the North Patagonian Andes. Synorogenic strata deposited in deltaic environment sourced from the east as part of a primitive contractional basin stage in the ARB. The latter would have developed in an attenuated crust before major orogenic load, lithospheric flexure and basin subsidence commonly described in relation to more advanced foreland basin stages.

A synthesis of Cretaceous deformation along the whole Andean Cordillera indicates that the Apeleg Formation potentially constitutes the oldest post-Gondwana synorogenic deposits of the Andes. More significantly, this synthesis and the obtained results reveal that Andean birth was a diachronic process that propagated northward. This pattern of initial deformation challenges current geodynamic models and sheds light into the driving process behind initial Andean subduction orogeny. We note that this particular evolution followed closely the path of South Atlantic Ocean opening and related changes in plate motion suggesting an origin directly linked to these processes. Subsequently, additional processes in Cenozoic times linked to an increase in upper plate motion, subduction length and depth, and slab age, as well as, climate change since Eocene times would have played a key role in producing the most significant deformation of the Andes.

Acknowledgements

The authors want to recognize the support received by CONICET and discussion with several members of the Laboratorio de Tectónica Andina and the Instituto Sismológico Ing. Fernando Volponi (IGSV) through the years. Also the U.S. National Science Foundation (NSF) grant EAR 1918541 awarded to B.K. Horton, and a NSF Graduate Research Fellowship awarded to K. Butler and PIP 2015-2017. nro 11220150100426 and UBACYT. 20020150100166BA. ubacyt 2015-2017 awarded to A. Folguera. We acknowledge PhD. Lucas Fennell, PhD. Maximiliano Naipauer and PhD. Matías Ghiglione for constructive comments and Associate Editor PhD. Damian Nance for effective handling of the manuscript. This is the R306 publication of IDEAN.

Appendix A. Supplementary data

Supplementary data to this article can be found online at https://doi.org/10.1016/j.gr.2019.07.014.

References

Aguirre-Urreta, B., Martinez, M., Schmitz, M., Lescano, M., Omarini, J., Tunik, M., Reboulet, S., 2019. Interhemispheric radio-astrochronological calibration of the time scales from the Andean and the Tethyan areas in the Valanginian-Hauterivian (Early Cretaceous). Gondwana Res. 70, 104–132.

Aguirre-Urreta, B., Ramos, V.A., 1981. Estratigrafía y paleontología de la alta cuenca de río Roble, Cordillera Patagónica. VIII Congreso Geológico Argentino. Actas III, In, pp. 101–138.

Aleman, A., Ramos, V.A., 2000. The northern Andes. In: Cordani, U.G., Milani, E.J., Thomaz Filho, A., Campos Neto, M.C. (Eds.), Tectonic Evolution of South America: 31st International Geological Congress. Institut de Recherche pour le Développement, Rio de Janeiro, Brazil, pp. 453–480.

Aramendía, I., Ramos, M.E., Geuna, S., Cuitiño, J.I., Ghiglione, M.C., 2018. A multidisciplinary study of the Lower Cretaceous marine to continental transition in the northern Austral-Magallanes basin and its geodynamic significance. J. S. Am. Earth Sci. 86, 54–69.

Armijo, R., Lacassin, R., Coudurier-Curveur, A., Carrizo, D., 2015. Coupled tectonic evolution of Andean orogeny and global climate. Earth Sci. Rev.143, 1–35.

Arriagada, C., Cobbold, P.R., Roperch, P., 2006. Salar de Atacama basin: a record of compressional tectonics in the central Andes since the mid-cretaceous. Tectonics 25, TC1008. doi:https://doi.org/10.1029/2004TC001770.

Auboin, J.A., Borrello, A.V., Cecione, G., Charrier, R., Chotin, P., Frutos, J., Thiele, R., Vicente, J.C., 1973. Esquisse paleogeographique et structurale des Andes meridionales. Rev. Geogr. Phys. Geol. 15, 11–71.

Baby, P., Rivadeneira, M., Barragán, R., 2004. La Cuenca Oriente: Geología y petróleo. Travaux de l'Institut Français des Etudes Andine 144, 295. https://horizon documentation.ird.fr/exl-doc/pleins_textes/doc34-08/010036207.pdf.

Baker, P.A., Fritz, S.C., Dick, C.W., Eckert, A.J., Horton, B.K., Manzoni, S., Battisti, D.S., 2014. The emerging field of geogenomics: constraining geological problems with genetic data. Earth Sci. Rev. 135, 38–47.

Baker, P.E., Rea, W.J., Skarmeta, J., Caminos, R., Rex, D.C., 1981. Igneous history of the Andean cordillera and Patagonian plateau around latitude 46°S. Philos. Trans. Royal Soc. 303 (1474), 105–149.

Balgord, E.A., Carrapa, B., 2016. Basin evolution of Upper Cretaceous–lower Cenozoic strata in the Malargüe fold-and-thrust belt: northern Neuquén Basin. Argentina. Basin Res. 28, 183–206.

Barnes, J.B., Ehlers, T.A., 2009. End member models for Andean Plateau uplift. Earth Sci. Rev. 97, 105–132.

Barragán, R., 1999. Relations entre volcanisme, tectonique d' inversión et sédimentation dans le bassin Crétacé Équatorien. [Ph.D. thesis]. Université Paul Sabatier, Toulouse, France (223 p).

Bascuñán, S., Arriagada, C., Le Roux, J., Deckart, K., 2016. Unraveling the Peruvian phase of the Central Andes: stratigraphy, sedimentology and geochronology of the Salar de Atacama Basin (22°30–23°S), northern Chile. Basin Res. 28, 365–392.

Bechis, F., Giambiagi, L., García, V., Lanés, S., Cristallini, E., Tunik, M., 2010. Kinematic analysis of a transtensional fault system: the Atuel depocenter of the Neuquén basin, southern Central Andes, Argentina. J. Struct. Geol. 32 (7), 886–899.

Bell, C.M., 2004. Asteroid and ophiuroid trace fossils from the Lower Cretaceous of Chile. Palaeontology 47, 51–66.

Bell, C.M., Súarez, M., 1997. The lower cretaceous Apeleg Formation of the Aisén basin, southern Chile. Tidal sandbar deposits of an epicontinental sea. Rev. Geol. Chile 24, 203–226.

Bhattacharya, J.P., 2006. Deltas. In: Posamentier, H., Walker, R.G. (Eds.), Facies Models Revisited: SEPM. 84, pp. 237–292 Special Publication.

Bhattacharya, J.P., Davies, R.K., 2001. Growth faults at the prodelta to delta front transition, cretaceous Ferron Sandstone. Utah. Mar. Petroleum Geol. 18, 525–534.

Biddle, K., Uliana, M., Mitchum Jr., R., Fitzgerald, M., Wright, R., 1986. In: Allen, P.A., Homewood, P. (Eds.), Foreland Basins. The stratigraphic and structural evolution of the central and eastern Magallanes Basin, southern South America, International Association of Sedimentologists Special Publication 8, 41–61.

Boyce, D.I., Charrier, R., Tapia, F., Farías, M., 2014. Mid-Cretaceous Compressive Deformation in Central Chile: The Beginning of the Andean Building (In AGU Fall Meeting Abstracts).

Braz, C., Seton, M., Flament, N., Müller, R.D., 2018. Geodynamic reconstruction of an accreted cretaceous back-arc basin in the Northern Andes. J. Geodyn. 121, 115–132.

Bruhn, R.L., Dalziel, I.W.D., 1977. In: Talwani, M., Pitman III, W.C. (Eds.), Island Arcs, Deep Sea Trenches, and Back-Arc Basins, Destruction of the early cretaceous marginal basin in the Andes of Tierra del Fuego. American Geophysical Union, Maurice Ewing Series 1, 395–405.

Brune, S., Williams, S.E., Butterworth, N.P., Müller, R.D., 2016. Abrupt plate accelerations shape rifted continental margins. Nature 536 (7615), 201.

Burbank, D., Meigs, A., Brozovic, N., 1996. Interactions of growing folds and coeval depositional systems. Basin Res. 8 (3), 199–224.

Butler, K.L., Horton, B.K., Echaurren, A., Folguera, A., Fuentes, F., 2019. Cretaceous-Cenozoic Growth of the Patagonian Broken Foreland Basin. Chronostratigraphic framework and provenance variations during transitions in Andean subduction dynamics. J S Am. Earth Sci, Argentina (in press).

Calderon, M., Prades, C.F., Herve, F., Avendaño, V., Fanning, C.M., Massonne, H.J., Theye, T., Simonetti, A., 2013. Petrological vestiges of the late Jurassic-early cretaceous transition from rift to back-arc basin in southernmost Chile: new age and geochemical data from the Capitán Aracena, Carlos III, and Tortuga ophiolitic complexes. Geochem. J. 47 (2), 201–217.

Capitanio, F.A., Faccenna, C., Zlotnik, S., Stegman, D.R., 2011. Subduction dynamics and the origin of Andean orogeny and the Bolivian orocline. Nature 480, 83–86. https://doi.org/10.1038/nature10596.

Chang, Z., Vervoort, D.J., Mcclelland, W.C., Knaack, C., 2006. U-Pb dating of zircon by LA-ICP-MS. Geochem. Geophys. Geosyst. 7 (5). https://doi.org/10.1029/2005GC001100.

Chappel, B., White, A., 2001. Two contrasting granite types: 25 years later. Aust. J. Earth Sci. 48, 489–499.

Charrier, R., Pinto, L., Rodríguez, M., 2007. In: Moreno, T., Gibbons, W. (Eds.), Tectonostratigraphic evolution of the Andean orogen in Chile. The Geology of Chile. J. Geol. Soc. 21–114.

Chen, Y.W., Wu, J., Suppe, J., 2019. Southward propagation of Nazca subduction along the Andes. Nature 565 (7740), 441.

Cobbold, P.R., Rossello, E.A., 2003. Aptian to recent compressional deformation of the Neuquén Basin. Argentina. Mar. Petroleum Geol. 20, 429–443.

Cobbold, P.R., Rossello, E.A., Roperch, P., Arriagada, C., Gómez, L.A., Lima, C., 2007. Distribution, timing, and causes of Andean deformation across South America. J. Geol. Soc. Spe. Pap. 272, 321–343.

Colwyn, D.A., Brandon, M.T., Hren, M.T., Hourigan, J.K., Pacini, A., Cosgrove, M., Midzic, M., Gerraud, R., Metzger, C.A., 2017. A Cenozoic Water Isotope Record of the Evolution of the Patagonian Andes (In AGU Fall Meeting Abstracts).

Coney, P.J., Evenchick, C.A., 1994. Consolidation of the American Cordilleras. J. S. Am. Earth Sci. 7, 241–262.

Cooper, M.A., Addison, F.T., Alvarez, R., Coral, M., Graham, R.H., Hayward, A.B., Howe, S., Martinez, J., Naar, J., Peñas, R., Pulham, A.J., Taborda, A., 1995. Basin development and tectonic history of the Llanos basin, Eastern Cordillera, and Middle Magdalena Valley. Colombia. Am. Assoc. Pet. Geol. Bull. 79, 1421–1443.

Cox, K.G., Bell, J.D., Pankhurst, R.J., 1979. The interpretation of igneous rocks. Allen, London, p. 450.

Dalziel, I.W.D., 1981. Back-arc extension in the southern Andes: a review and critical reappraisal. Philos. Trans. Royal Soc. A 300, 319–355.

Dalziel, I.W.D., 1986. In: Coward, M.P., Ries, A.C. (Eds.), Collision Tectonics. Collision and cordillera orogenesis: an Andean perspective. J. Geol. Soc. Spe. Pap. 19, 389–404.

Dalziel, I.W.D., de Wit, M.J., Palmer, K.F., 1974. Fossil marginal basin in the southern Andes. Nature 250 (5464), 291–294.

DeCelles, P.G., 2012. Foreland basin systems revisited: Variations in response to tectonic settings. Tectonics of sedimentary basins: Recent advances 405–426.

Decelles, P.G., Zandt, G., Beck, S., Currie, C.A., Ducea, M.N., Kapp, P.A., ... Schoenbohm, L.M., 2015. Cyclical orogenic processes in the Cenozoic central Andes. Geol. Soc. Am. Mem. 212, 459–490.

Demant, A., González, M.S., 2010. Early cretaceous Surtseyan volcanoes of the Baño Nuevo volcanic complex (Aysén Basin, Eastern Central Patagonian Cordillera, Chile). Geol. Acta 8 (2), 207–219.

Demant, A., Suárez, M., De La Cruz, R., 2007. Lower cretaceous surtseyan volcanoes in the Eastern central Patagonian Cordillera (45°15′– 45°40′S): the Baño Nuevo volcanic complex. An international Congress on the Geology and Geophysics of the Southern Hemisphere-Geosur, 18–20 November 2007, Santiago, Chile, 51.

DePaolo, D.J., Harrison, T.M., Wielicki, M., Zhao, Z., Zhu, D.C., Zhang, H., Mo, X., 2019. Geochemical evidence for thin syn-collision crust and major crustal thickening between 45 and 32 Ma at the southern margin of Tibet. Gondwana Res. 73, 123–135.

Depine, G.V., Ramos, V.A., 2004. Geología de la quebrada Honda, cuenca del lago La Plata. Chubut. Rev. Asoc. Geol. Argent. 59 (4), 643–654.

Di Giulio, A., Ronchi, A., Sanfilippo, A., Tiepolo, M., Pimentel, M., Ramos, V.A., 2012. Detrital zircon provenance from the Neuquén Basin (south-Central Andes): cretaceous geodynamic evolution and sedimentary response in a retroarc-foreland basin. Geology 40, 559–562.

Di Giulio, A., Ronchi, A., Sanfilippo, A., Balgord, E.A., Carrapa, B., Ramos, V.A., 2016. Cretaceous evolution of the Andean margin between 36 S and 40 S latitude through a multi-proxy provenance analysis of Neuquén Basin strata (Argentina). Basin Res. https://doi.org/10.1111/bre.12176.

Dickinson, W.R., 1983. Provenance of North American Phanerozoic sandstones in relation to tectonic setting. Geol. Soc. Am. Bull. 94, 222–257. https://doi.org/10.1130/0016-7606(1983)94<222:PONAPS>2.0.CO;2.

Domínguez, E., 1981. Génesis y geoquímica de la mineralización de los yacimientos Los Manantiales y Lago Fontana, provincia del Chubut. Rev. Asoc. Geol. Argent. 36 (2), 123–142.

Echaurren, A., Folguera, A., Gianni, G., Orts, D., Tassara, A., Encinas, A., Giménez, M., Valencia, V., 2016. Tectonic evolution of the north Patagonian Andes (41°–44° S) through recognition of syntectonic strata. Tectonophysics 677, 99–114.

Echaurren, A., Oliveros, V., Folguera, A., Ibarra, F., Creixell, C., Lucassen, F., 2017. Early Andean tectonomagmatic stages in North Patagonia: insights from field and geochemical data. J. Geol. Soc. https://doi.org/10.1144/jgs2016-087.

EXXON Petroleum Company, 1988. The EXXON 'Global' Sea-level Curve (unpublished).

Faccenna, C., Oncken, O., Holt, A.F., Becker, T.W., 2017. Initiation of the Andean orogeny by lower mantle subduction. Earth Planet. Sci. Let. 463, 189–201.

Farías, M., D. Comte, R. Charrier, J. Martinod, C. David, A. Tassara, F. Tapia, and A. Fock (2010). Crustal-scale structural architecture in Central Chile based on seismicity and surface geology: Implications for Andean mountain building. Tectonics 29, TC3006, doi:https://doi.org/10.1029/2009TC002480.

Fennell, L.M., Folguera, A., Naipauer, M., Gianni, G., Rojas Vera, E., Bottesi, G., Ramos, V.A., 2015. Cretaceous deformation of the southern Central Andes: Synorogenic growth strata in the Neuquén Group (35°30′–37°S). Basin Res. 29, 51–72.

Fildani, A., Hessler, A.M., 2005. Stratigraphic record across a retroarc basin inversion: Rocas Verdes–Magallanes Basin, Patagonian Andes. Chile. Geol. Soc. Am. Bull. 117, 1596–1614. https://doi.org/10.1130/B25708.1.

Fildani, A., Cope, T.D., Graham, S.A., Wooden, J.L., 2003. Initiation of the Magallanes foreland basin: timing of the southernmost Patagonian Andes orogeny revised by detrital zircon provenance analysis. Geology 31, 1081–1084.

Finch, E., Hardy, S., Gawthorpe, R., 2004. Discrete-element modeling of extensional fault-propagation folding above rigid basement fault blocks. Basin Res. 16 (4), 467–488.

Folguera, A., Iannizzotto, N.F., 2004. The Lagos La Plata and Fontana fold-and-thrust belt: long-lived orogenesis at the edge of western Patagonia. Geol. SJ. S. Am. Earth Sci. 16, 541–566.

Folk, R.L., Andrews, P.B., Lewis, D., 1970. Detrital sedimentary rock classification and nomenclature for use in New Zealand. New Zeal. J. Geol. 13 (4), 937–968.

Fuentes, G., Martínez, F., Bascuñan, S., Arriagada, C., Muñoz, R., 2018. Tectonic architecture of the Tarapacá Basin in the northern Central Andes: New constraints from field and 2D seismic data. Geosphere. https://doi.org/10.1130/GES01697.1.

Garzione, C.N., Molnar, P., Libarkin, J.C., MacFadden, B.J., 2006. Rapid late Miocene rise of the Bolivian Altiplano: evidence for removal of mantle lithosphere. Earth Planet. Sci. Let. 241 (3), 543–556.

Gawthorpe, R., Hardy, S., 2002. Extensional fault-propagation folding and base-level change as controls on growth-strata geometries. Sediment. Geol. 146 (1–2), 47–56.

Gazzi, P., 1966. Le minerali pesanti nei flysch arenacei fra Monte Ramaceto e Monte Molinatico (Appennino settent Ríonale). Mineral. Petrogr. Acta 11, 197–212.

Gehrels, G., Pecha, M., 2014. Detrital zircon U-Pb geochronology and Hf isotope geochemistry of Paleozoic and Triassic passive margin strata of western North America. Geosphere. 10, 49–65.

Gehrels, G.E., Valencia, V.A., Pullen, A., 2006. Detrital zircon geochronology by laser-ablation multicollector ICPMS at the Arizona LaserChron Center. Paleontol. Soc. Pap. 12, 67.

Gehrels, G. E., Valencia, V. A., Ruiz, J., 2008. Enhanced precision, accuracy, efficiency, and spatial resolution of U-Pb ages by laser ablation–multicollector–inductively coupled plasma–mass spectrometry. Geochem., Geophys., Geosyst. 9(3).

Ghiglione, M.C., Likerman, J., Giambiagi, L.B., Aguirre-Urreta, B., Suarez, F., 2014. Geodynamic context for the deposition of coarse-grained deep-water axial channel systems in the Patagonian Andes. Basin Res. 26, 726–745.
Ghiglione, M.C., Naipauer, M., Sue, C., Barberón, V., Valencia, V., Aguirre-Urreta, M.B., Ramos, V.A., 2015. U-Pb zircon ages from the northern Austral basin and their correlation with the Early Cretaceous exhumation and volcanism of Patagonia. Cretac. Res. 55, 116–128.
Ghiglione, M.C., Ramos, V., Cuitiño, J., Barberón, V., 2016. Growth of the Southern Patagonian Andes (46–53°S) and its relation with subduction processes. In: Folguera, A., Naipauer, M., Sagripanti, L., Ghiglione, M.C., Orts, D.L., Giambiagi, L. (Eds.), Growth of the Southern Andes. Springer, Berlin, pp. 201–240.
Giambiagi, L., Mescua, J., Bechis, F., Martínez, A., Folguera, A., 2011. Pre-Andean deformation of the Precordillera southern sector, southern Central Andes. Geosphere 7 (1), 219–239.
Giambiagi, L., Mescua, J., Bechis, F., Tassara, A., Hoke, G., 2012. Thrust belts of the southern Central Andes: Along-strike variations in shortening, topography, crustal geometry, and denudation. Geol. Soc. Am. Bull. 124 (7–8), 1339–1351.
Gianni, G., Navarrete, C., Orts, D., Tobal, J., Folguera, A., Giménez, M., 2015. Patagonian broken foreland and related synorogenic rifting: the origin of the Chubut Group Basin. Tectonophysics 649, 81–99.
Gianni, G.M., Echaurren, A., Folguera, A., Likerman, J., Encinas, A., García, H.P.A., Dal Molin, C., Valencia, V.A., 2017. Cenozoic intraplate tectonics in Central Patagonia: record of main Andean phases in a weak upper plate. Tectonophysics 721, 151–166.
Gianni, G.M., Navarrete, C., Liendo, I., Díaz, M., Giménez, M.E., Encinas, A., Folguera, A., 2018a. Cretaceous Intraplate Contraction in Southern Patagonia: A Far-Field Response to Changing Subduction Dynamics? Tectonics 37 (9), 2915–2937.
Gianni, G.M., Dávila, F.M., Echaurren, A., Fennell, L., Tobal, J., Navarrete, C., Quezada, P., Folguera, A., Giménez, M., 2018b. A geodynamic model linking cretaceous orogeny, arc migration, foreland dynamic subsidence and marine ingression in southern South America. Earth Scienci. Rev. 185, 437–462.
Gómez, E., Jordan, T.E., Allmendinger, R.W., Hegarty, K., Kelley, S., Heizler, M., 2003. Controls on architecture of the Late Cretaceous to Cenozoic southern Middle Magdalena Valley Basin. Colombia. Geol. Soc. Am. Bull. 115, 131–147.
Gómez, E., Jordan, T.E., Allmendinger, R.W., Cardozo, N., 2005. Development of the Colombian foreland-basin system as a consequence of diachronous exhumation of the northern Andes. Geol. Soc. Am. Bull. 117, 1272–1292.
Gómez, R., Lothari, L., Tunik, M., Casadio, S., 2019. Onset of foreland basin deposition in the Neuquén Basin (34°-35° S). New data from sedimentary petrology and U–Pb dating of detrital zircons from the Upper Cretaceous non-marine deposits. J South Am. Earth Sci. 102257.
González-Bonorino, G., Suárez, G., 1995. Paleoambientes sedimentarios de la Formación Apeleg, Cretácico Inferior de la Cuenca de Aisén, Región XI. Chile. Rev. Geol. Chile 22 (1), 115–126.
Groeber, P., 1946. Observaciones geológicas a lo largo del meridiano 70°. Hoja Chos Malal. Rev. Soc. Geol. Arg. 1, 178–208.
Groeber, P., 1947. Observaciones geológicas a lo largo del meridiano 70°. 3 Hojas Domuyo, Mari Mahuida, Huarhuar-co y parte de Epu Lauken. Rev. Soc. Geol. Arg. 2(4): 347-408. Buenos Aires. 70.
Hallam, A., Cohen, J., 1989. The case for sea-level change as a domi- nant causal factor in mass extinction of marine invertebrates [and discussion]. Phil. Trans. R. Soc. B. (Biological Sciences) London 325, 437–455.
Haq, B., Hardenbol, J., Vail, P., 1987. Chronology of fluctuating sea levels since the Triassic. Science 235, 1156–1167.
Hechem, J.J., Figari, E., Homovc, J., 1993. Secuencias deposicionales en el Neocomiano del Lago Fontana, Chubut, Argentina. XII Congreso Geológico Argentino (Mendoza). Actas 2, 119–123.
Heine, C., Brune, S., 2014. Oblique rifting of the Equatorial Atlantic: why there is no Saharan Atlantic Ocean? Geology 42 (3), 211–214.
Heuret, A., Lallemand, S., 2005. Plate motions, slab dynamics and back-arc deformation. Phys. Earth Planet. Inter. 149 (1-2), 31–51.
Hong, F., del Papa, C., Powell, J., Petrinovic, I., Mon, R., Deraco, V., 2007. Middle Eocene deformation and sedimentation in the Puna-Eastern Cordillera transition (23 S–26 S): Control by preexisting heterogeneities on the pattern of initial Andean shortening. Geology 35 (3), 271–274. https://doi.org/10.1130/G23189A.1.
Hoorn, C., Wesselingh, F.P., Ter Steege, H., Bermudez, M.A., Mora, A., Sevink, J., ... Jaramillo, C., 2010. Amazonia through time: Andean uplift, climate change, landscape evolution, and biodiversity. Science 330 (6006), 927–931.
Horton, B.K., 2018a. Sedimentary record of Andean mountain building. Earth Sci. Rev. 178, 279–309.
Horton, B.K., 2018b. Tectonic regimes of the central and southern Andes: responses to variations in plate coupling during subduction. Tectonics 37. https://doi.org/10.1002/2017TC004624.
Horton, B.K., Hampton, B.A., Waanders, G., 2001. Paleogene synorogenic sedimentation in the Altiplano plateau and implications for initial mountain building in the central Andes. Geol. Soc. Am. Bull. 113, 1387–1400.
Horton, B.K., Saylor, J.E., Nie, J., Mora, A., Parra, M., Reyes-Harker, A., Stockli, D.F., 2010. Linking sedimentation in the northern Andes to basement configuration, Mesozoic extension, and Cenozoic shortening: evidence from detrital zircon U-Pb ages, Eastern Cordillera. Colombia. Geol. Soc. Am. Bull. 122, 1423–1442.
Hu, F., Ducea, M.N., Liu, S., Chapman, J.B., 2017. Quantifying crustal thickness in continental collisional belts: global perspective and a geologic application. Sci. Rep. 7 (1), 7058.
Hurtado, C., Roddaz, M., Santos, R.V., Baby, P., Antoine, P.O., Dantas, E.L., 2018. Cretaceous-early Paleocene drainage shift of Amazonian rivers driven by Equatorial Atlantic Ocean opening and Andean uplift as deduced from the provenance of northern Peruvian sedimentary rocks (Huallaga basin). Gondwana Res. 63, 152–168.
Husson, L., Conrad, P.C., Faccenna, C., 2012. Plate motions, Andean orogeny, and volcanism above the South Atlantic convection cell. Earth Planet. Sci. Let. 317–318, 126–135.
Iannizzotto, N.F., Folguera, A., Leal, P.R., 2004. Control tectónico de las secuencias volcaniclásticas neocomianas y paleogeografía en la zona del Lago La Plata (45°S). Sector interno de la faja plegada y corrida de los lagos La Plata y Fontana. Rev. Asoc. Geol. Argent. 59, 655–670.
Jaillard, E., Soler, P., 1996. Cretaceous to early Paleogene tectonic evolution of the northern Central Andes (0-18°S) and its relations to geodynamics. Tectonophysics 259 (1–3), 41–53. https://doi.org/10.1016/0040-1951(95)00107-7.
Jaillard, E., Hérail, G., Monfret, T., Díaz-Martínez, E., Baby, P., Lavenu, A., Dumont, J.F., 2000. In: Cordani, U.G., Milani, E.J., Thomaz Filho, A., Campos Neto, M.C. (Eds.), Tectonic evolution of the Andes of Ecuador, Peru, Bolivia and northernmost Chile. Tectonic Evolution of South America: 31st International Geological Congress. Brazil, Rio de Janeiro, pp. 481–559.
Jaimes, E., Freitas, M., 2006. An Albian-Cenomanian unconformity in the northern Andes: evidence and tectonic significance. J. S. Am. Earth Sci. 21 (4), 466–492. https://doi.org/10.1016/j.jsames.2006.07.011.
Kay, S.M., Mpodozis, C., Ramos, V.A., Munizaga, F., 1991. In: Harmon, R. S., Rapela, C. W. (Eds), Magma source variations for mid-late Tertiary magmatic rocks associated with a shallowing subduction zone and a thickening crust in the Central Andes (28 to 33°S). Andean Magmatism and its Tectonic setting. Geol. Soc. Am. Spe. Pap. 265, 113–137.
Kennan, L., Pindell, J.L., 2009. Dextral shear, terrane accretion and basin formation in the Northern Andes: best explained by interaction with a Pacific-derived Caribbean Plate? J. Geol. Soc. Spe. Pub. 328, 487–531. https://doi.org/10.1144/SP328.20.
Kohn, M.J., Spear, F.S., Harrison, T.M., Dalziel, I.W.D., 1995. 40Ar/39Ar geochronology and P-T-t paths from the Cordillera Darwin metamorphic complex, Tierra del Fuego, Chile. J. Metamorph. Geol. 13, 251–270.
Lamb, S., Davis, P., 2003. Cenozoic climate change as a possible cause for the rise of the Andes. Nature 425, 792–797. https://doi.org/10.1038/nature02049.
Lanfranchini, M., Curci, M., Etcheverry, R., Marchionni, D., 1999. Mineralización Epitermal (Au-Ag) en Estancia Pepita, Provincia del Chubut. República Argentina. Studia Geologica Salmanticensia 35.
López-Blanco, M., Marzo, M., Muñoz, J.A., 2003. Low-amplitude, synsedimentary folding of a deltaic complex: Roda Sandstone (lower Eocene), South-Pyrenean Foreland Basin. Basin Res. 15 (1), 73–96.
Ludwig, K. R., 2003. ISOPLOT 3.0, a geochronological toolkit for microsoft excel: Berkeley Geochronology Center special publication, no. 4, Berkeley.
Malkowski, M.A., Sharman, G.R., Graham, S.A., Fildani, A., 2015. Characterization and diachronous initiation of coarse clastic deposition in the Magallanes–Austral retroarc foreland basin. Patagonian Andes. Basin Res. https://doi.org/10.1111/bre.12150.
Malkowski, M.A., Grove, M., Graham, S.A., 2016. Unzipping the Patagonian Andes—Long-lived influence of rifting history on foreland basin evolution. Lithosphere 8 (1), 23–28.
Malkowski, M.A., Schwartz, T.M., Sharman, G.R., Sickmann, Z.T., Graham, S.A., 2017. Stratigraphic and provenance variations in the early evolution of the Magallanes-Austral foreland basin: Implications for the role of longitudinal versus transverse sediment dispersal during arc-continent collision. Geol. Soc. Am. Bull. 129 (3–4), 349–371.
Martin-Gombojav, N., Winkler, W., 2008. Recycling of Proterozoic crust in the Andean Amazon foreland of Ecuador: implications for orogenic development of the Northern Andes. Terra Nova 20 (1), 22–31.
Martínez, F., Arriagada, C., Valdivia, R., Deckart, K., Peña, M., 2015. Geometry and kinematics of the Andean thick-skinned thrust systems: insights from the Chilean Frontal Cordillera (28–28.5 S), Central Andes. J. South Am. Earth Sci. 64, 307–324.
Martínez, F., Arriagada, C., Bascuñán, S., 2018a. In: Folguera et al. (Eds), Mechanisms and episodes of deformation along the Chilean–Pampean flat-slab Subduction Segment of the Central Andes in Northern Chile. The evolution of the Chilean-Argentinean Andes 273-290. Springer, Cham.
Martínez, F., López, C., Bascuñan, S., Arriagada, C., 2018b. Tectonic interaction between Mesozoic to Cenozoic extensional and contractional structures in the Preandean Depression (23°–25° S): Geologic implications for the Central Andes. Tectonophysics 744, 333–349.
McAtamney, J., Klepeis, K., Mehrtens, C., Thomson, S., Betka, P., Rojas, L., and Snyder, S., 2011, Along-strike variability of back-arc basin collapse and the initiation of sedimentation in the Magallanes foreland basin, southernmost Andes (53–54.5°S): Tectonics 30, 5. TC5001, doi:https://doi.org/10.1029/2010TC002826.
McDonough, W.F., Sun, S.S., 1995. The composition of the Earth. Chem. Geol. 120, 223–253.
Mégard, F., 1984. The Andean orogenic period and its major structures in central and northern Peru. J. Geol. Soc. 141, 893–900.
Menegazzo, M.C., Catuneanu, O., Chang, H.K., 2016. The South American retroarc foreland system: the development of the Bauru Basin in the back-bulge province. Mar. Petroleum Geol. 73, 131–156.
Mora, A., Baby, P., Roddaz, M., Parra, M., Brusset, S., Hermoza, W., Espurt, N., 2010. In: Hoorn, C., Wesselingh, F.P. (Eds.), Amazonia: Landscape and Species Evolution: A Look Into the Past. Tectonic History of the Andes and sub-Andean Zones: Implications for the Development of the Amazon Drainage Basin. Wiley-Blackwell, Chichester, UK, pp. 38–60 https://doi.org/10.1002/9781444306408.ch4.
Mosquera, A., Ramos, V.A., 2006. Intraplate deformation in the Neuquén Basin. In: Kay, S.M., Ramos, V.A. (Eds.), Evolution of an Andean margin: a Tectonic and Magmatic View from the Andes to the Neuquén Basin (35°–39°S Latitude): Geol. Soc. Am. Spe. Pap. 407, 97–124.
Mpodozis, C., Ramos, V.A., 1990. The Andes of Chile and Argentina. In: Ericksen, G.E., Cañas Pinochet, M.T., Reinemund, J.A. (Eds.), Geology of the Andes and its Relation to Hydrocarbon and Mineral Resources. Circum-Pacific Council for Energy and Mineral Resources. Earth Sci. Series vol. 11, pp. 59–90.

Mpodozis, C., Arriagada, C., Basso, M., Roperch, P., Cobbold, P., Reich, M., 2005. Late Mesozoic to Paleogene stratigraphy of the Salar de Atacama Basin, Antofagasta, northern Chile: Implications for the tectonic evolution of the Central Andes. Tectonophysics 399, 125–154.

Mulch, A., Uba, C.E., Strecker, M.R., Schoenberg, R., Chamberlain, C.P., 2010. Late Miocene climate variability and surface elevation in the Central Andes. Earth Planet. Sci. Let. 290, 173–182.

Müntener, O., Ewing, T., Baumgartner, L.P., Manzini, M., Roux, T., Pellaud, P., Alleman, L., 2018. Source and fractionation controls on subduction-related plutons and dike swarms in southern Patagonia (Torres del Paine area) and the low Nb/Ta of upper crustal igneous rocks. Contributions Mineral. Petrol. 173, 38. https://doi.org/10.1007/s00410-018-1467-0.

Nakamura, N., 1974. Determination of REE, Ba, Fe, Mg, Na, and K in carbonaceous and ordinary chondrites. Geochim. Cosmochim. Acta 38, 757–775.

Navarro, E.L., Astini, R.A., Belousova, E., Guler, M.V., Gehrels, G., 2015. Detrital zircon geochronology and provenance of the Chubut Group in the northeast of Patagonia, Argentina. J. S. Am. Earth Sci. 63, 149–161.

Nelson, E.P., Dalziel, I.W.D., Milnes, A.G., 1980. Structural geology of the Cordillera Darwin; collisional-style orogenesis in the southernmost Chilean Andes. Eclogae Geol. Helv. 73, 727–751.

Nie, J., Horton, B.K., Mora, A., Saylor, J.E., Housh, T.B., Rubiano, J., Naranjo, J., 2010. Tracking exhumation of Andean ranges bounding the Middle Magdalena Valley Basin, Colombia. Geology 38, 451–454.

Nivia, A., Marriner, G.F., Kerr, A.C., Tarney, J., 2006. The Quebradagrande complex: A lower cretaceous ensialic marginal basin in the Central Cordillera of the Colombian Andes. J. S. Am. Earth Sci. 21, 423–436.

Nürnberg, D., Müller, R.D., 1991. The tectonic evolution of the South Atlantic from Late Jurassic to present. Tectonophysics 191, 27–53. https://doi.org/10.1016/0040-1951(91)90231-G.

Olivero, E., Aguirre-Urreta, M., 2002. Sucesión de amonoideos de la Formación Katterfeld (Valanginiano-Hauteriviano) en su área tipo, Lago Fontana, Chubut, XV Congreso Geolo´gico Argentino (El Calafate), electronic book.

Oncken O, Hindle D, Kley J, Elger K, Victor P, Schemmann K, 2006. In: Oncken O et al., (Eds.)., Deformation of the Central Andean upper plate system—Facts, fiction, and constraints for plateau models. The Andes, Springer Berlin Heidelberg 22:3–27.

Orts, D.L., Folguera, A., Encinas, A., Ramos, M., Tobal, J., Ramos, V.A., 2012. Tectonic development of the North Patagonian Andes and their related Miocene foreland basin (41°30′–43° S). Tectonics 31, 1–24.

Paces, J.B., Miller, J.D., 1993. Precise U-Pb ages of Duluth complex and related mafic intrusions, northeastern Minnesota: Geochronological insights to physical, petrogenetic, paleomagnetic, and tectonomagmatic processes associated with the 1.1 Ga midcontinent rift system. J. Geophys. Res. Solid Earth 98 (B8), 13997–14013.

Pankhurst, R., Riley, T., Fanning, C., Kelley, S., 2000. Episodic silicic volcanism in Patagonia and the Antartic Península: chronology of magmatism associated with the break-up of Gondwana. J. Petrol. 41 (5), 605–625.

Pankhurst, R.J., Hervé, F., Fanning, M., Suárez, M., 2003. Coeval plutonic and volcanic activity in the Patagonian Andes: the Patagonian Batholith and the Ibánez and Divisadero Formations, Aisén, southern Chile. In: Congreso Geológico Chileno No. 10. Actas CD-ROM. Concepción. Chile.

Pearce, J.A., Harris, N.B., Tindle, A.G., 1984. Trace element discrimination diagrams for the tectonic interpretation of granitic rocks. J. Petrol. 25 (4), 956–983.

Peccerillo, A., Taylor, S.R., 1976. Geochemistry of Eocene calc-alkaline volcanic rocks from the Kastamonu area, northern Turkey. Contrib. Mineral. Petrol. 58 (1), 63–81.

Pfiffner, O., Gonzalez, L., 2013. Mesozoic-Cenozoic evolution of the western margin of South America: case study of the Peruvian Andes. Geosciences 3 (2), 262.

Pindell, J.L., Kennan, L., 2009. Tectonic evolution of the Gulf of Mexico, Caribbean and northern South America in the mantle reference frame: an update. J. Geol. Soc. Spe. Pub. 328 (1), 1–55.

Ploszkiewicz, J., Ramos, V.A., 1987. Estratigrafía y tectónica de la Sierra de Payaniyeu, provincia de Chubut. Rev. Asoc. Geol. Argent. 32, (3–4).

Poulsen, C.J., Ehlers, T.A., Insel, N., 2010. Onset of convective rainfall during gradual Late Miocene rise of the Central Andes. Science 328 (5977), 490–493. http://dx.doi.

Ramos, M.E., Geuna, S., Aramendia, I., Maffione, M., Boixart, G., Ramos, Ghiglione M., V. A., 2016. Constraints on the tectonic evolution of the Patagonian southern Andes in Santa Cruz from anisotropy of magnetic susceptibility and structural data (46°–48°S). Paper Presented at 1° International Symposium on South American Tectonics. Chile, Santiago.

Ramos, V.A., 1981a. Descripción geológica de la hoja 47 ab Lago Fontana, Provincia de Chubut. Servicio Geológico Nacional. Bol., Buenos Aires. vol. 183. pp. 130.

Ramos, V.A., 1981b. Descripción geológica de la Hoja 33c Los Chihuidos Norte, Provincia del Neuquén. Servicio Geológico Nacional, Boletín 182, 1–103 Buenos Aires.

Ramos, V.A., 2008. Patagonia: a Paleozoic continent adrift? J. S. Am. Earth Sci. 26, 235–251.

Ramos, V.A., 2009. Anatomy and global context of the Andes: Main geologic features and the Andean orogenic cycle. Backbone of the Americas: shallow subduction, Plateau Uplift, and Ridge and Terrane collision. Geol. Soc. Am. Mem. 204, 31–65.

Ramos, V.A., Palma, M., 1983. Las Lutitas pizarreñas fosilíferas del Cerro Dedo y su evolución tectónica; Lago La Plata. Provincia de Chubut. Rev. Asoc. Geol. Argent. 38 (2), 148–160.

Rapela, C.W., Pankhurst, R.J., Fanning, C.M., Hervé, F., 2005. In: Vaughan, A.P.M., Leat, P.T., Pankhurst, R.J. (Eds.) Terrane Accretion Processes at the Pacific Margin of Gondwana, Pacific subduction coeval with the Karoo mantle plume: the Early Jurassic Subcordilleran Belt of northwestern Patagonia. J. Geol. Soc. 246, 217–239.

Restrepo, J.J., Toussaint, J.F., 1991. Terranes and continental Acretion in the Colombian Andes. Episodes 11 (3), 189–193.

Reyes, F.C., 1972. Correlaciones en el Cretacico de la Cuenca Andina de Bolivia, Peru y Chile. Revista Técnica YPF B 1 (2), 101–144.

Reyes-Harker, A., Ruiz-Valdivieso, C.F., Mora, A., Ramírez-Arias, J.C., Rodriguez, G., de la Parra, F., Caballero, V., Parra, M., Moreno, N., Horton, B.K., Saylor, J.E., Silva, A., Valencia, V., Stockli, D., Blanco, V., 2015. Cenozoic paleogeography of the Andean foreland and retroarc hinterland of Colombia. AAPG Bull. 99, 1407–1453.

Riba, O., 1976. Syntectonic unconformities of the Alto Cardener. Spanish Pyrenees: a genetic interpretation. Sediment Geol. 15, 213–233.

Riesner, M., Lacassin, R., Simoes, M., Carrizo, D., Armijo, R., 2018. Revisiting the crustal structure and kinematics of the Central Andes at 33.5 S: Implications for the mechanics of Andean mountain building. Tectonics 37 (5), 1347–1375.

Rolando, A., Hartmann, L., Santos, J.O., Fernandez, R., Etcheverry, R., Schalamuk, I., McNaughton, N., 2002. SHRIMP zircon U–Pb evidence for extended Mesozoic magmatism in the Patagonian Batholith and assimilation of Archean crustal components. Geol. SJ. S. Am. Earth Sci. 15, 267–283.

Ronda, G., Ghiglione, M.C., Barberón, V., Coutand, I., Tobal, J., 2019. Mesozoic-Cenozoic evolution of the Southern Patagonian Andes fold and thrust belt (47°-48°S): Influence of the Rocas Verdes basin inversion and onset of Patagonian glaciations. Tectonophysics https://doi.org/10.1016/j.tecto.2019.05.009.

Ruiz, G.M.H., 2002. Exhumation of the Northern Sub-Andean Zone of Ecuador and Its Source Region: A Combined Thermochronological and Heavy Mineral Approach. [Ph.D. thesis]. Institute of Geology, ETH Zürich, Switzerland 132 p. https://www.research-collection.ethz.ch/handle/20.500.11850/147228.

Scasso, R., 1989. In: Chebli, G., Spalletti, L.A. (Eds.), Cuencas Sedimentarias Argentinas, La cuenca sedimentaria del Jurásico Superior y Cretácico Inferior de la región sudoccidental de Chubut. Serie de Correlación Geológica 6, Instituto Superior de Correlación Geológica 395–417.

Scasso, R. A., 1987. Estratigrafía y ambientes de sedimentación del ciclo sedimentario del Jurásico superior y Cretácico inferior de la región sudoccidental del Chubut, con referencias a la columna estratigráfica general del área. PhD Thesis, University of Buenos Aires, 300 p.

Schellart, W.P., 2017. Andean mountain building and magmatic arc migration driven by subduction-induced whole mantle flow. Nature Comm. 8 (1), 2010.

Schiller, W., 1912. La Alta Cordillera de San Juan y Mendoza y parte de la provincia de San Juan. Ministerio de Agricultura de la Nación. Sección Geología. Mineralogía y Minería. Anales VII (5): 1-68. Buenos Aires. 7 (5), 1–68.

Sempere, T., 1995. Phanerozoic evolution of Bolivia and adjacent regions. In: Suárez Soruco, R., Welsink, H.J. (Eds.), Tankard, A.J. Petroleum Basins of South America, AAPG Bull, pp. 207–230.

Sempere, T., Butler, R.F., Richards, D.R., Marshall, L.G., Sharp, W., Swisher, C.C., 1997. Stratigraphy and chronology of upper cretaceous lower Paleogene strata in Bolivia and Northwest Argentina. Geol. Soc. Am. Bull. 109 (6), 709–727. https://doi.org/10.1130/0016-7606(1997)109<0709:SACOUC>2.3.CO;2.

Shand, S.J., 1943. The Eruptive Rocks. 2nd edition. John Wiley, New York.

Sharman, G.R., Sharman, J.P., Sylvester, Z., 2018. detritalPy: A Python-based toolset for visualizing and analyzing detrital geo-thermochronologic data. The Depositional Record. 202–215.

Sickmann, Z.T., Schwartz, T.M., Malkowski, M.A., Dobbs, S.C., and Graham, S.A., 2019. Interpreting Large Detrital Geochronology Data Sets in Retroarc Foreland Basins: An Example from the Magallanes-Austral Basin, Southernmost Patagonia. Lithosphere (in press)

Silver, P.G., Russo, R.M., Lithgow-Bertelloni, C., 1998. Coupling of South American and African plate motion and plate deformation. Science 279 (5347), 60–63.

Sláma, J., et al., 2008. Plešovice zircon — A new natural reference material for U–Pb and Hf isotopic microanalysis. Chem. Geol. 249 (1–2), 1–35. https://doi.org/10.1016/j.chemgeo.2007.11.005.

Somoza, R., Zaffarana, C.B., 2008. Mid-Cretaceous Polar Standstill of South America, Motion of the Atlantic Hotspots and the Birth of the Andean Cordillera. Earth Planet Sci. Let. 271, 267–277.

Spikings, R., Cochrane, R., Villagómez, D., Van der Lelij, R., Vallejo, C., Winkler, W., Beate, B., 2015. The geological history of northwestern South America: from Pangaea to the early collision of the Caribbean large Igneous Province (290–75 Ma). Gondwana Res. 27, 95–139.

Steinmann, G., 1929. Geologie von Perú. C. Winter, Heidelberg, p. 448.

Strecker, M.R., Hilley, G.E., Bookhagen, B., Sobel, E.R., 2011. Structural, geomorphic, and depositional characteristics of contiguous and broken foreland basins: examples from the eastern flanks of the central Andes in Bolivia and NW Argentina. Tectonics of sedimentary basins: Recent advances, pp. 508–521.

Suárez, M., De la Cruz, R., 2001. Jurassic to Miocene K-Ar dates from eastern central Patagonian Cordillera plutons, Chile (45–48 S). Geol. Mag. 138, 53–66.

Suárez, M., Márquez, M., 2007. A Toarcian retro-arc basin of Central Patagonia (Chubut), Argentina: Middle Jurassic closure,arc migration and tectonic setting. Rev. Geol Chile 34 (1). https://doi.org/10.4067/S0716-02082007000100004.

Suárez, M., De La Cruz, R. Bell, M., 1996. Estratigrafía de la región de Coyhaique (45°–46° latitud S); Cordillera Patagonica, Chile. In: Congreso Geologico Argentino No. 13 y Congreso de Exploracion de Hidrocarburos No. 3, 575–90. Buenos Aires.

Suárez, M., De La Cruz, R., Bell, M., Demant, A., 2009a. Cretaceous slab segmentation in southwestern Gondwana. Geol. Mag. 147, 193–205.

Suárez, M., Márquez, M., De La Cruz, R., Fanning, M., 2009b. Aptian-Albian subaerial volcanic rocks in central Patagonia: Divisadero and Chubut Groups. XII Congreso Geológico Chileno, In, pp. 1–4.

Suarez, M., Demant, A., De La Cruz, R., Fanning, C.M., 2010. 40Ar/39Ar and U-Pb SHRIMP dating of Aptian tuff cones in the Aisén Basin, Central Patagonian Cordillera. J. S. Am. Earth Sci. 29 (3), 731–737.

Suppe, J., Sàbat, F., Munoz, J.A., Poblet, J., Roca, E., Vergés, J., 1997. Bed-by-bed fold growth by kink-band migration: Sant Llorenç de Morunys, eastern Pyrenees. J. Struct. Geol. 19 (3-4), 443–461.

Thompson, R., Morrison, M., Hendry, G., Parry, S., 1984. An assessment of the relative roles of crust and mantle in magma genesis: an elemental approach. Phil. Trans. Royal Society London A 310, 549–590.
Tunik, M., Folguera, A., Naipauer, M., Pimentel, M., Ramos, V.A., 2010. Early uplift and orogenic deformation in the Neuquén Basin: Constraints on the Andean uplift from U-Pb and Hf isotopic data of detrital zircons. Tectonophysics, 489, 258–273.
Tunik, M.A., Vietto, M.E., Sciutto, J.C., 2004. Procedencia de areniscas del Grupo Chubut en el área central de la Sierra de San Bernardo. Análisis preliminar. Rev. Asoc. Geol. Argent. 59, 601–606.
Uliana, M. A., K. T. Biddle, J. Cerdan, A. J. Tankard, H. R. Balkwill, 1989. Mesozoic extension and the formation of Argentine sedimentary basins, In: H. J.Tankard (Ed.), Extensional tectonics and stratigraphy of the North Atlantic margins. AAPG 46, 599–614.
Uyeda, S., Kanamori, H., 1979. Back-arc opening and the mode of subduction. J. Geophys. Res. Solid Earth 84 (B3), 1049–1061.
Vallejo, C., 2007. Evolution of the Western Cordillera in the Andes of Ecuador (Late Cretaceous–Paleogene). [pH.D. thesis]. Institute of Geology. ETH Zürich, Switzerland, p. 208. https://www.research-collection.ethz.ch/handle/20.500.11850/150007.
Vérard, C., Hochard, C., Baumgartner, P.O., Stampfli, G.M., Liu, M., 2015. 3D palaeogeographic reconstructions of the Phanerozoic versus sea-level and Sr-ratio variations. J. Palaeog. 4 (1), 64–84.
Vicente, J.C., 1970. Reflexiones sobre la porción meridional del sistema peripacífico oriental, in Conferencia sobre Problemas de la Tierra Sólida: Buenos Aires. Proyecto Internacional del Manto Superior 37-I, 162–188.
Villagómez, D., Spikings, R., 2013. Thermochronology and tectonics of the Central and Western Cordilleras of Colombia: Early Cretaceous–Tertiary evolution of the Northern Andes. Lithos 160–161, 228–249.
Villagómez, D., Spikings, R., Magna, T., Kammer, A., Winkler, W., Beltrán, A., 2011. Geochronology, geochemistry and tectonic evolution of the Western and Central cordilleras of Colombia. Lithos 125, 875–896. https://doi.org/10.1016/j.lithos.2011.05.003.
Wilson, T.J., 1991. Transition from back-arc to foreland basin development in the southernmost Andes: Stratigraphic record from the Ultima Esperanza District, Chile. Geol. Soc. Am. Bull. 103, 98–111. https://doi.org/10.1130/0016-7606 (1991)103<0098:TFBATF>2.3.CO;2.
Yang, T., Moresi, L., Gurnis, M., Liu, S., Sandiford, D., Williams, S., Capitanio, F.A., 2019. Contrasted East Asia and South America tectonics driven by deep mantle flow. Earth Planet. Sci. Lett. 517, 106–116.
Zapata, S., Cardona, A., Jaramillo, J.S., Patiño, A., Valencia, V., León, S., Mejía, D., Pardo-Trujillo, A., Castañeda, J.P., 2019. Cretaceous extensional and compressional tectonics in the Northwestern Andes, prior to the collision with the Caribbean oceanic plateau. Gondwana Res. 66, 207–226.
Zuffa, G.G., 1985. Optical analyses of arenites: influence of methodology on compositional results. Provenance of arenites. Springer, Dordrecht, pp. 165–189.